Journal of Hydrology 633 (2024) 130982

Contents lists available at ScienceDirect

Journal of Hydrology

journal homepage: www.elsevier.com/locate/jhydrol

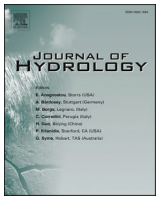

Influence of Pleistocene glacial deposits on the transport of agricultural nitrate in the river Wensum catchment, UK

Kevin M. Hiscock [a,*], Richard J. Cooper [a], Melinda A. Lewis [b], Daren C. Gooddy [b], Thomas J. Howson [c], Sarah K. Wexler [a,d]

[a] School of Environmental Sciences, University of East Anglia, Norwich Research Park, Norwich NR4 7TJ, UK
[b] British Geological Survey, Maclean Building, Wallingford OX10 8BB, UK
[c] RPS (A Tetra Tech Company), Pentagon House, Sir Frank Whittle Road, Derby DE21 4XA, UK
[d] Institute of Archaeology, University College London, Gordon Square, London WC1H 0PY, UK

ARTICLE INFO

This manuscript was handled by Huaming Guo, Editor-in-Chief, with the assistance of Huaming Guo, Associate Editor

Keywords:
Pleistocene glacial deposits
Agriculture
Groundwater nitrate
Stable isotopes
Groundwater residence time indicators
Storm hydrograph separation

ABSTRACT

Mitigating NO_3^- pollution requires an understanding of the hydrological processes controlling contaminant mobilisation and transport, particularly in agricultural catchments underlain by Pleistocene glacial deposits. Focusing on the Wensum catchment in East Anglia, UK, precipitation ($n = 20$), stream water ($n = 50$), field drainage ($n = 22$) and groundwater ($n = 84$) samples collected between February–March 2011 and April–September 2012 were variously analysed for water stable isotopes (δ^2H_{H2O} and $\delta^{18}O_{H2O}$), the dual-isotopes of NO_3^- ($\delta^{15}N_{NO3}$ and $\delta^{18}O_{NO3}$), groundwater residence time indicators (CFCs and SF_6) and hydrochemical parameters. The residence time indicators suggested a component of modern (post-1960) groundwater throughout the sequence of glacial deposits that corresponds with the penetration of agricultural NO_3^-. Denitrification and lower NO_3^- concentrations (<8 mg L^{-1}) are observed in the glacial tills, compared with higher NO_3^- concentrations (<90 mg L^{-1}) observed under more oxidising conditions in the glacial sands and gravels. Storm hydrograph separation for two storms in April and September 2012 using two- and three-component mixing models showed a faster response with field drainage (36–38 %) and baseflow (5–37 %) contributing to the total stream discharge in areas of clay loam soils over glacial tills. In these areas, the dual stable isotopes of NO_3^- ($\delta^{15}N_{NO3} = +11.8$ ‰ and $\delta^{18}O_{NO3} = +7.1$ ‰) indicated a denitrified source of nitrogen from field drainage and groundwater. In comparison, a dampened response and a higher percentage of baseflow (29–80 %) was observed in areas of sandy clay loam soils over glacial sands and gravels. In these areas, mean NO_3^- isotopic signatures ($\delta^{15}N_{NO3} = +7.8$ ‰ and $\delta^{18}O_{NO3} = +5.0$ ‰) indicated a source of nitrified NH_4^+. In conclusion, understanding hydrological processes in catchments underlain by variable glacial deposits can inform nutrient management plans and cultivation practices to reduce the risk of agricultural NO_3^- contamination.

1. Introduction

Potential contaminants such as inorganic and organic fertilisers, pesticides and veterinary products used in agriculture can reach groundwater along diffuse pathways via direct infiltration or as more focused point source runoff (Burri et al., 2019; Gros et al., 2021; Warrack et al., 2022; Bradley et al., 2023; Cui et al., 2023). Specifically, the large increase in global nitrogen production and use has improved global food security but with detrimental impacts on greenhouse gas emissions (Gao and Cabrera Serrenho, 2023), human health (Wolfe and Patz, 2002; Patel et al., 2022) and the environment (Kopáček et al., 2013; Webster et al., 2021; Yuan et al., 2023). Elevated levels of reactive nitrogen cause eutrophication, hypoxia events, loss of biodiversity and habitat degradation in freshwater and coastal ecosystems (Steffen et al., 2015; Wurtsbaugh et al., 2019; Sekar et al., 2022; Zhang et al., 2022).

Achieving reductions in agricultural pollution within river basins requires changes in land management and the implementation of mitigation measures to tackle the principal reasons for water quality failure (Hiscock et al., 2023). Underpinning the design of effective pollution mitigation strategies is an understanding of the hydrological functioning of catchments, particularly in relation to the way in which catchments store, mix and release water and the dynamics of pollutant mobilisation

* Corresponding author.
E-mail address: k.hiscock@uea.ac.uk (K.M. Hiscock).

https://doi.org/10.1016/j.jhydrol.2024.130982
Received 6 October 2023; Received in revised form 19 January 2024; Accepted 6 February 2024
Available online 28 February 2024

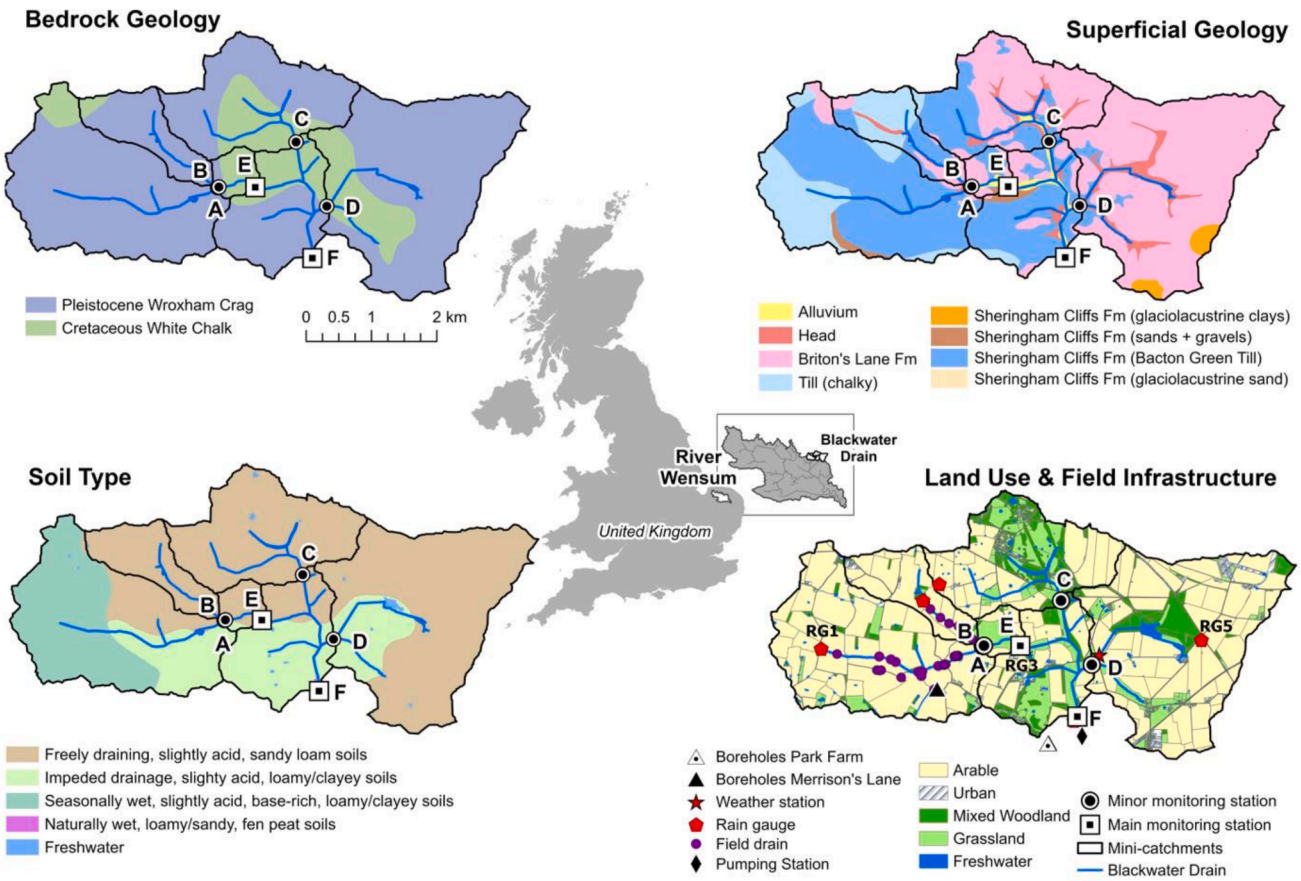

Fig. 1. Spatial variability in bedrock geology (BGS; GSI3D model), superficial geology (BGS; GSI3D model), land use (LCM2015; Rowland et al., 2017) and soil type (LandIS; Cranfield Soil and Agrifood Institute Soilscapes) across the Blackwater Drain sub-catchment of the River Wensum, UK. Also shown are the positions of the field monitoring infrastructure and mini-catchment boundaries. Geological maps reproduced with the permission of the British Geological Survey, ©UKRI. Based upon Land Cover Map 2015 © UKCEH 2017. Contains Ordnance Survey data © Crown Copyright 2007, Licence number 100017572. .
Adapted from Cooper et al. (2018)

and transport under a range of hydrometeorological and hydrogeological conditions (Cooper et al., 2018; Peskett et al., 2023).

Catchments with underlying glacial deposits are important hydrogeological environments that often support productive agricultural regions, particularly in the northern latitudes of North America, northern Europe and Scandinavia that experienced widespread glaciation throughout the Pleistocene Epoch (Kehew and Teller, 1994; Houmark-Nielsen, 2010; Ferris et al., 2020). As a result of repeated cycles of glacial advance followed by glacial retreat and warmer interglacial periods, glacial deposits are characterised by heterogeneous sedimentary assemblages with a wide range of hydraulic properties and variable lateral extent (Ferris et al., 2020).

The heterogeneity of glacial deposits is a challenge in catchment management given the complex patterns of groundwater flow that impact groundwater and surface water interactions (Fleckenstein et al., 2006; Kawo et al., 2023). Often, glacial deposits are composed of clay-rich tills that form aquitard units, an understanding of which is necessary in the context of a variety of catchment processes (van der Kamp, 2001; Cuthbert et al., 2010; Hendry et al., 2016; Neuzil, 2019). Previous research has shown that glacial tills commonly exhibit hydraulically conductive fracture networks, embedded sand and gravel lenses and extensive weathering of the near-surface deposits (Hiscock and Tabatabai Najafi, 2011; Kessler et al., 2012, 2013; Ferris et al., 2020). Hence, a better understanding of local glacial geology and how it impacts the spatial variability of subsurface characteristics will enable the implementation of more targeted catchment management practices (Best et al., 2015).

The aim of this research is to examine the role of Pleistocene glacial deposits in influencing the partitioning of runoff and agricultural NO_3^- in surface water and groundwater in the Wensum catchment in Norfolk, East Anglia. Two methodological approaches are employed: (i) analysis of stable isotopes (δ^2H_{H2O} and $\delta^{18}O_{H2O}$), residence time indicators and hydrochemical data for different components of the hydrological system (precipitation, field drainage, pore water and pumped groundwater from the glacial deposits, and groundwater from the underlying Chalk aquifer); and (ii) storm hydrograph analysis of stream discharge using stable isotopes, including the dual-isotopes of NO_3^- ($\delta^{15}N_{NO3}$ and $\delta^{18}O_{NO3}$), and corroborating hydrochemical data. The research presented here is applicable to other agricultural regions underlain by Pleistocene glacial deposits and is intended to inform catchment management practices to reduce the water quality impact and economic cost of agricultural NO_3^- contamination (Sutton et al., 2021; Garcia-Hernandez et al., 2022; Cooper and Hiscock, 2023; Husic et al., 2023).

2. Study area and experimental methods

2.1. Study area

The River Wensum is a 78 km long, lowland calcareous river in Norfolk with a catchment area of 660 km^2 (52°47′09″N, 01°07′00″E) (Fig. 1) and mean annual discharge of 4.1 m^3/s near its outlet (UKCEH, 2023). Annual baseflow indices (BFI) range from 0.75 in the lower part of the catchment where the underlying Cretaceous Chalk aquifer is confined by superficial Pleistocene glacial deposits, to 0.82 in the upper

Table 1
Completion details for the Merrison's Lane (Site A) and Park Farm (Site F) groundwater monitoring borehole installations, including depth of water strikes recorded during drilling and groundwater levels in May 2012.

Borehole ID	British Grid Reference (TG)	Flange top elevation (m OD)	Depth (m)	Internal diameter (mm)	Slotted casing (m)	Depth of water strike (m)	Water level 01/05/12 (m OD)	Completed in
Merrison's Lane (Site A)								
A4	10369 25018	42.98	4.00	50	1.0–3.6	–	42.41	Bacton Green Till Member (chalk-clasts in a clay/silt matrix)
A3	10384 25011	43.17	12.02	50	5.0–12.0	4.8	41.18	Sheringham Cliffs Formation (glacial sands)
A2	10373 25015	43.00	15.26	50	12.3–15.3	4.5, 14.7	41.50	Lowestoft Till Member (chalk clasts in a clay/silt matrix)
A1	10379 25017	43.17	46.53	74	25.0–50.0	5.1, 16.3, 21.5	39.90	Chalk
Park Farm (Site F)								
F4	12071 24185	39.12	6.38	50	1.3–6.0	4.7	33.28	Briton's Lane Formation (sand and gravel)
F3	12081 24191	39.34	10.13	74	8.0–10.0	4.8	32.19	Sheringham Cliffs Formation (glacial sands)
F2	12079 24200	39.40	16.41	50	12.5–16.5	5.1	31.46	Happisburgh Formation (sand and gravel)
F1	12073 24190	39.23	44.63	74	24.1–47.7	4.8, 11.6, 17.2	31.34	Chalk

part of the catchment where the Chalk outcrops. The area experiences a temperate maritime climate, with a mean annual temperature of 10.5 °C and a mean annual precipitation total of 684 mm (1991–2020) (Meteorological Office, 2023).

The Wensum catchment is divided into several sub-catchments, including the 19.7 km^2 Blackwater Drain that is the focus of this study (Fig. 1). For monitoring purposes, this sub-catchment is further divided into mini-catchments A–F. Mini-catchments A (5.38 km^2) and B (1.34 km^2) drain the western area of the sub-catchment and mini-catchments C (3.52 km^2) and D (6.61 km^2) the northern and eastern areas. Mini-catchment E monitors higher-order stream flow downstream of mini-catchments A and B. The total flow from the sub-catchment is monitored at Site F with BFI values in the range 0.69–0.74 for the hydrological years 2012–2014 (Outram et al., 2016). Land use in the Blackwater sub-catchment is predominantly arable (75 %), with some improved grassland and fresh water (13 %), mixed woodland (10 %) and rural settlements (2 %) (Rowland et al., 2017).

The bedrock geology in the Blackwater sub-catchment is Cretaceous Chalk (>20 m thickness) and Pleistocene Wroxham Crag (sand and gravel; 0–23.5 m thickness) overlain by a variable succession of superficial deposits comprising Mid-Pleistocene chalky, flint-rich, argillaceous glacial tills of the Sheringham Cliffs Formation (Bacton Green Till Member; 22 m maximum thickness) and Lowestoft Formation (Lowestoft Till Member; 38 m maximum thickness), with interdigitated bands of glaciofluvial and glaciolacustrine sands and gravels (Lewis, 2014; Cooper et al., 2018). Soils developed on the glacial deposits are predominantly clay loam to sandy clay loam (<0.5 m depth) of the argillic brown earths (Freckenham series) and stagnogley (Beccles series) groups which, together with the argillaceous tills, result in moderately impeded drainage conditions.

The western part of the Blackwater sub-catchment is underlain by glacial tills and clay-rich, poorly draining soils. Much of this area is extensively under-drained by a dense network of agricultural tile drains (43 km^{-1}) installed at depths of 100–160 cm below ground level (bgl). Measured drain discharges are typically < 0.2 L/s, although can be as high as 10 L/s during the winter and dry up entirely during the summer (June–September), with discharge also varying greatly depending upon depth, catchment area and antecedent moisture conditions (Hama-Aziz et al., 2017). The eastern part of the sub-catchment is underlain by glacial sands and gravels that are more freely draining with well drained sandy loam soils. The mean slope in the sub-catchment is 1.2° with minimum and maximum elevations of 25.3 and 70.2 m above sea level, respectively.

2.2. *Field methods*

At the six Blackwater monitoring stations (Sites A–F), bankside stations were installed for the purpose of water sampling and river water quality monitoring. River stage at each monitoring station was measured using pressure transducers housed in stilling wells (Impress IMSL Submersible Level Transmitter) and converted into river discharge via stage-discharge rating curves constructed from manual flow gauging with an open-channel EM flow meter (Outram et al., 2014, 2016). Precipitation amount was recorded at locations distributed across the study area (Fig. 1) using Casella tipping bucket rain gauges, with a resolution of 0.2 mm depth of water.

Storm event sampling of surface waters at monitoring stations A and D was undertaken using Teledyne ISCO automatic water samplers programmed to collect 1 L samples at hourly intervals. Samples were retrieved from the field the following day to avoid evaporation affecting samples for stable isotope analysis. Precipitation samples were collected every three to four days using a standard rain gauge located at monitoring station E (gauge RG3), with the gauge completely emptied and dried prior to redeployment. Samples were decanted from the ISCO samplers and rain gauge into 50 mL HDPE bottles and returned to cold storage prior to analysis.

Grab samples from field drain outflows (see Fig. 1 for locations) were collected in 1 L polypropylene bottles and returned to the laboratory for analysis. Groundwater samples from the two borehole installations at Merrison's Lane ('Site A' located 875 m southwest of the monitoring

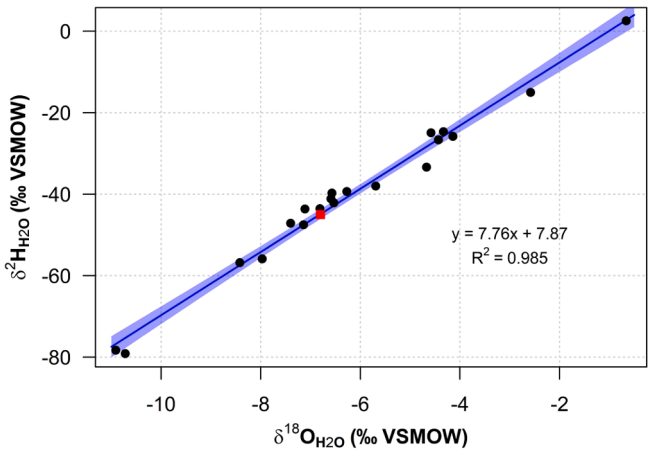

Fig. 2. δ^2H_{H2O} versus $\delta^{18}O_{H2O}$ relationship for precipitation collected from April–June 2012 in the Blackwater sub-catchment showing the Local Water Meteoric Line (LMWL): $\delta^2H_{H2O} = 7.76\ \delta^{18}O_{H2O} + 7.87$. See also Table 2 for mean and weighted mean values of the water stable isotopes. Shading around the linear regression line is the 95 % confidence interval and the red square represents the volume-weighted mean isotopic composition of sampled precipitation. (For interpretation of the references to colour in this figure legend, the reader is referred to the web version of this article.)

station in mini-catchment A) and Park Farm ('Site F' located 600 m southwest of the monitoring station at the sub-catchment outlet) (Fig. 1) were obtained using either a peristaltic or submersible electrical pump depending on the rate of groundwater inflow.

Four boreholes were drilled in February and March 2011 at each of the Merrison's Lane (Site A) and Park Farm (Site F) locations by percussive drilling with a shell and auger rig and included a deep borehole (c. 50 m depth) into the Cretaceous Chalk and three shallower boreholes (c. 6, 12 and 15 m depths) in the overlying glacial deposits (Lewis, 2014). The two deepest boreholes into the superficial deposits (boreholes A2 and F2) were cored for lithological logging and pore water extraction. During drilling, 100 mm (U100 or U4) diameter core samples with a nominal length of 0.5 m were taken. Details of the completed boreholes including location references, lithology, drilled depth, depth intervals of slotted casing, depth of water strikes and example water levels are given in Table 1. Details of the centrifugation and mechanical squeezing methods used for pore water extraction from the core samples are given in the Supplementary Material (SM).

Groundwater samples were collected in September 2011 shortly after the boreholes had been developed by pumping, except for borehole F4 that could not be developed sufficiently to provide a yield of water. In addition to the borehole sampling at Sites A and F, a further Chalk groundwater sample was collected in September 2011 from Salle Pumping Station located 550 m east of Park Farm (Site F) (Fig. 1). A second round of pumped groundwater samples was collected in June 2012 in the same field season as the field drain survey and surface water sampling. Groundwater samples for CFC and SF_6 analysis were collected unfiltered and without atmospheric contact in glass bottles contained within metal cans by the displacement method of Oster et al. (1996). This method ensures that the sample is protected from possible atmospheric contamination by a jacket of the same water (Gooddy et al., 2006).

2.3. Laboratory methods

2.3.1. Hydrochemical analyses

Surface water and pumped groundwater samples were analysed by the Science Analytical Facilities at the University of East Anglia (UEA), Norwich and the Analytical Geochemistry Laboratory at the British Geological Survey (BGS), Keyworth to determine concentrations of nutrients and major ions using standard analytical methods. Details of the analytical methods and detection limits are given in the SM.

2.3.2. Water stable isotopes

Measurement of $\delta^{18}O_{H2O}$ and δ^2H_{H2O} by the UEA Stable Isotope Laboratory used a Picarro L1102–i liquid water isotope analyser with a precision of ±0.25 ‰ for $\delta^{18}O_{H2O}$ and ±2 ‰ for δ^2H_{H2O}. Additional stable isotope analysis of pore water and groundwater samples from the two borehole installations at Sites A and F were undertaken in the Stable Isotope Laboratory at BGS, Wallingford using an Optima dual inlet isotope ratio mass spectrometer with a precision of ±0.1 ‰ for $\delta^{18}O_{H2O}$ and ±1 ‰ for δ^2H_{H2O}. Details of the standards used for the water stable isotope analysis are given in the SM.

2.3.3. Dual stable isotopes of nitrate

Measurement of the dual stable isotopes of NO_3^- ($\delta^{15}N_{NO3}$ and $\delta^{18}O_{NO3}$) in the UEA Stable Isotope Laboratory followed the well-established denitrifier method (Sigman et al., 2001; Casciotti et al., 2002) and analysis on a Europa Geo 20:20 GC-IRMS with a TG II prep system with a mean measurement error of ±0.2 ‰ for $\delta^{15}N_{NO3}$ and ±0.4 ‰ for $\delta^{18}O_{NO3}$. The standards used for the analysis of the dual stable isotopes of NO_3^- are given in the SM.

2.3.4. Residence time indicators

Residence time indicators (CFC-11, CFC-12 and SF_6) were analysed at BGS, Wallingford by gas chromatography with an electron capture detector after pre-concentration by cryogenic methods, based on the procedures of Oster et al. (1996) and Busenberg and Plummer (2000). The detection limit of CFC-11 and CFC-12 concentrations in water was 0.01 pmol/L, and for SF_6 was 0.1 fmol L^{-1}.

2.4. Hydrograph separation

Isotopic and chemical hydrograph separation techniques have been widely applied to determine stream flow components in various catchments under different environmental conditions (Ogunkoya and Jenkins, 1991; Durand et al., 1993; Ladouche et al., 2001; Williams and McAfee, 2021; Gospodyn et al., 2023). The technique is based on a two or three-component mixing model representing conservation of mass describing the amount of water and environmental tracers from precipitation (surface runoff or event water) and groundwater (pre-event water) in the stream hydrograph of the event. The mass balance equations describing two- and three-component stream water mixing are given in the SM.

In this study, $\delta^{18}O_{H2O}$ is used as an environmental tracer to explore the partitioning of stream flow components during a storm event in April 2012. A two-component mixing model is used to examine the hydrological response in mini-catchment D. Given the presence of field drainage in mini-catchment A, a three-component mixing model is applied with $\delta^{18}O_{H2O}$ and NO_3^- chosen as the two environmental tracers. Although NO_3^- is not a conservative parameter, both NO_3^- and $\delta^{18}O_{H2O}$ are chemically distinguishable and demonstrate contrasting end-member components suitable for application in the mixing model. In addition, a second storm event in September 2012 was sampled for the stable isotopes of NO_3^- to investigate sources and processes affecting NO_3^- in stream discharge. For this event, given that the field drains were not running at the end of the summer baseflow recession period, a two-component mixing model is used with SO_4^{2-} as the tracer to examine the hydrological response in both mini-catchments A and D. For both storm events, Cl^- was found to be an unsuitable tracer due to elevated surface water concentrations, possibly due to an additional non-agricultural source such as road runoff, as found for fluvial sediment sources (Cooper et al., 2015a).

Table 2
Stable isotope and hydrochemical data for the Blackwater sub-catchment collected in February–March 2011, September 2011 and April–June 2012. The locations of the rain gauge, field drains in mini-catchment A, and the Merrison's Lane (Site A), Park Farm (Site F) and Salle Pumping Station (PS) boreholes are shown in Fig. 1. Electrical conductivity measurements are adjusted to 25 °C. Pumped groundwater samples are shown as collected at the mid-point of the slotted casing intervals in metres below ground level (m bgl).

Sample type	Sample ID	Date	Measurement	$\delta^{18}O_{H2O}$ (‰)	$\delta^{2}H_{H2O}$ (‰)	Conductivity (μS cm^{-1})	HCO_3^- (mg L^{-1})	Cl^- (mg L^{-1})	NO_3^- (mg L^{-1})	SO_4^{2-} (mg L^{-1})	PO_4^{2-} (μg L^{-1})
Precipitation	RG3	03/04/12–16/06/12	Mean (1σ)	−6.18 (2.39)	−40.0 (18.7)			3.49 (2.17)	0.73 (0.51)	2.22 (1.25)	
(*n* = 20)			Wt. mean	−6.81	−45.2	–	–	3.16	0.75	2.01	–
			Min	−10.91	−79.1	–	–	0.95	0.25	0.70	–
			Max	−0.66	2.5	–	–	7.96	1.92	5.69	–
Field drains:	A	30/04/12–01/05/12	Mean (1σ)	−6.95 (0.20)	−45.6 (2.6)	414 (95)	339 (78)	54.5 (22.7)	67.9 (54.3)	41.8 (22.0)	97 (233)
Mini-catchment A			Median	−6.93	−45.1	444	354	60.9	45.8	36.1	11
(*n* = 22)			Min	−7.47	−56.2	78	65	11.0	7.8	5.6	2
			Max	−6.60	−42.7	528	464	91.9	202	102	1051
Pore water:	A	02–03/11	Mean (1σ)	−7.20 (0.31)	−47.9 (2.1)	–	214 (109)	48.8 (25.7)	2.41 (2.68)	69.2 (45.4)	–
			Median	−7.11	−47.6	–	194	48.0	0.69	58.0	–
Site A			Min	−7.89	−52.8	–	75	14.0	<0.02	7.1	<100
(*n* = 35)			Max	−6.62	−43.6	–	446	117.2	7.88	183.0	211
	F	02–03/11	Mean (1σ)	−7.38 (0.34)	−49.1 (2.2)	–	166 (109)	39.5 (18.6)	30.3 (30.9)	59.4 (36.1)	–
Site F			Median	−7.34	−49.2	–	179	32.1	15.6	56.9	–
(*n* = 33)			Min	−8.22	−54.1	–	5	16.6	1.3	10.4	<100
			Max	−6.72	−44.1	–	381	80.4	92.3	121.0	251
Pumped groundwater:	A4	8–9/09/11	2.3 m bgl	−7.38	−49.9	941	469	29.8	<0.02	101	<100
	A3	8–9/09/11	8.5 m bgl	−7.10	−46.5	785	405	30.1	1.31	54.1	<100
Site A	A2	8–9/09/11	13.8 m bgl	−7.22	−47.4	945	432	62.3	0.26	44.2	<100
(*n* = 8)	A1 (Chalk)	8–9/09/11	37.5 m bgl	−7.17	−45.6	754	367	36.2	0.07	37.4	<100
	F3	8–9/09/11	9.0 m bgl	−7.50	−49.2	747	344	14.3	65.2	32.3	<200
Site F	F2	8–9/09/11	14.5 m bgl	−7.87	−51.1	1027	382	79.2	30.9	91.7	<100
(*n* = 7)	F1 (Chalk)	8–9/09/11	35.9 m bgl	−7.56	−48.2	799	394	42.6	0.08	41.1	<100
	A4	19/06/12	2.3 m bgl	−7.85	−50.9	487	550	20.8	0.13	47.3	51
Salle PS	A3	18/06/12	8.5 m bgl	−7.27	−47.0	432	412	25.1	0.71	45.1	6
(*n* = 1)	A2	18/06/12	13.8 m bgl	−7.35	−48.4	385	519	17.1	<0.01	43.6	31
	A1 (Chalk)	18/06/12	37.5 m bgl	−7.50	−49.6	376	415	31.2	0.53	28.3	59
	F4	19/06/12	3.7 m bgl	−7.36	−46.3	325	281	11.0	45.1	42.8	56
	F3	19/06/12	9.0 m bgl	−7.50	−49.5	504	364	11.5	53.9	26.1	18
	F2	19/06/12	14.5 m bgl	−7.54	−49.2	504	384	61.2	31.5	79.7	12
	F1 (Chalk)	19/06/12	35.9 m bgl	−7.53	−47.7	381	392	33.4	<0.01	22.7	53
	Salle PWS (Chalk)	08/09/11	49.3 m bgl	−7.43	−50.4	906	302	73.5	27.6	98.6	<100

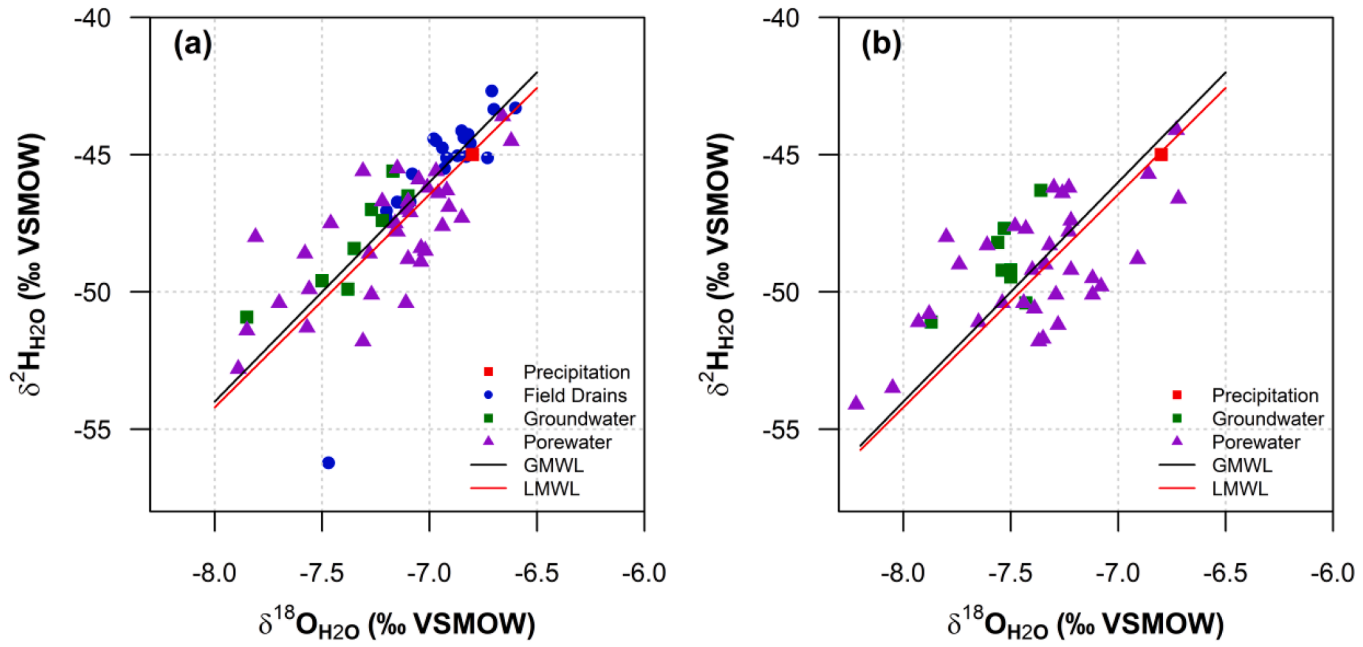

Fig. 3. δ^2H_{H2O} versus $\delta^{18}O_{H2O}$ relationship for: (a) field drainage, pumped groundwater and pore water obtained for mini-catchment A and Merrison's Lane (Site A) boreholes; and (b) pumped groundwater and pore water obtained for Park Farm (Site F) boreholes. Also shown are the Global Meteoric Water Line (GMWL) ($\delta^2H_{H2O} = 8\ \delta^{18}O_{H2O} + 10$) and Local Water Meteoric Line (LWML) ($\delta^2H_{H2O} = 7.76\ \delta^{18}O_{H2O} + 7.87$). The red square represents the volume-weighted mean isotopic composition of sampled precipitation. (For interpretation of the references to colour in this figure legend, the reader is referred to the web version of this article.)

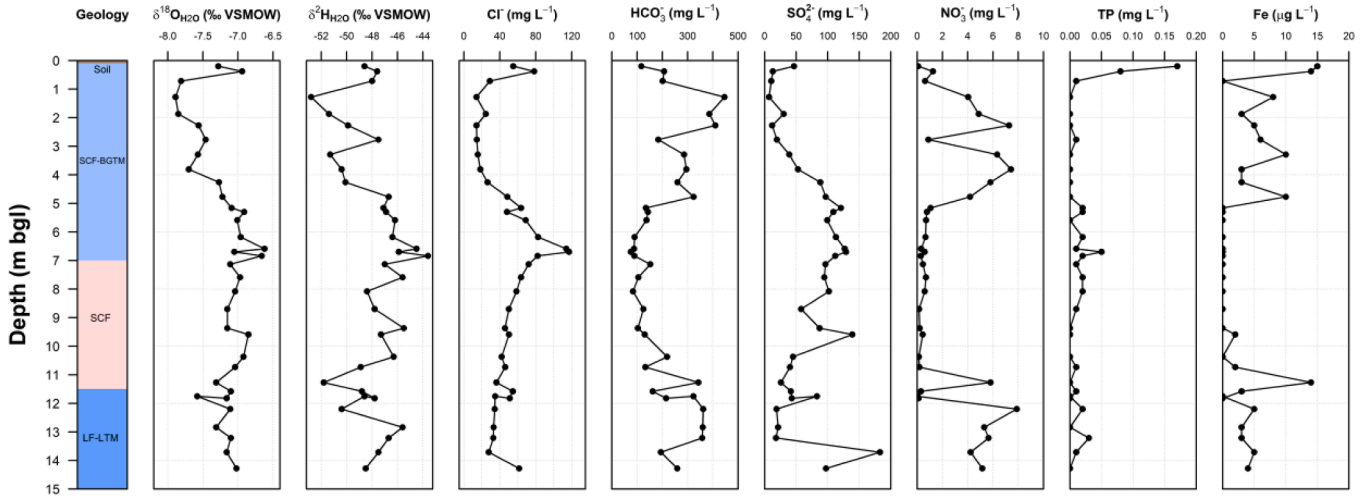

Fig. 4. Vertical stable isotope and hydrochemical profiles for pore waters extracted from glacial deposits at Site A (Merrison's Lane borehole A2). See Fig. 1 for borehole location. Geological nomenclature: SCF, Sheringham Cliffs Formation; BGTM, Bacton Green Till Member; LF, Lowestoft Formation; LTM, Lowestoft Till Member. Based on Lewis (2014) © Crown copyright and database rights 2014. (For interpretation of the references to colour in this figure legend, the reader is referred to the web version of this article.)

3. Results and discussion

3.1. Water stable isotope data

Fig. 2 shows the δ^2H_{H2O} versus $\delta^{18}O_{H2O}$ relationship for precipitation collected during the warmer spring/summer months of April–June 2012, with the variation in values reflecting temperature effects on both the condensation and isotopic fractionation of meteoric water. The linear regression equation ($\delta^2H_{H2O} = 7.76\ \delta^{18}O_{H2O} + 7.87$) represents the Local Meteoric Water Line (LMWL) and is comparable to the Global Meteoric Water Line (GMWL) ($\delta^2H_{H2O} = 8\ \delta^{18}O_{H2O} + 10$) (Craig, 1961). In the interpretation of groundwater isotopic compositions, the volume-weighted mean isotopic composition of precipitation is taken to represent the isotopic signature of the seasonal recharge, with values of $\delta^{18}O_{H2O} = -6.8$ ‰ and $\delta^2H_{H2O} = -45$ ‰ obtained for this study (Table 2). These values compare with isotopically more depleted compositions of $\delta^{18}O_{H2O} = -7.2$ ‰ and $\delta^2H_{H2O} = -48$ ‰ for the volume-weighted mean isotopic composition of cooler, winter precipitation for the hydrological year 1995–1996 obtained by George (1998) for a rain gauge at the nearby Salle Pumping Station.

Stable isotope data for precipitation, field drainage, pore water and pumped groundwater samples collected in the Blackwater sub-catchment in September 2011 and April–June 2012 are presented in Table 2 and Fig. 3. The $\delta^{18}O_{H2O}$ compositional ranges for field drainage (−7.5 to −6.6 ‰) and pumped groundwater from Merrison's Lane (Site A) (−7.9 to −7.3 ‰) (Fig. 3a) represent two statistically different groups

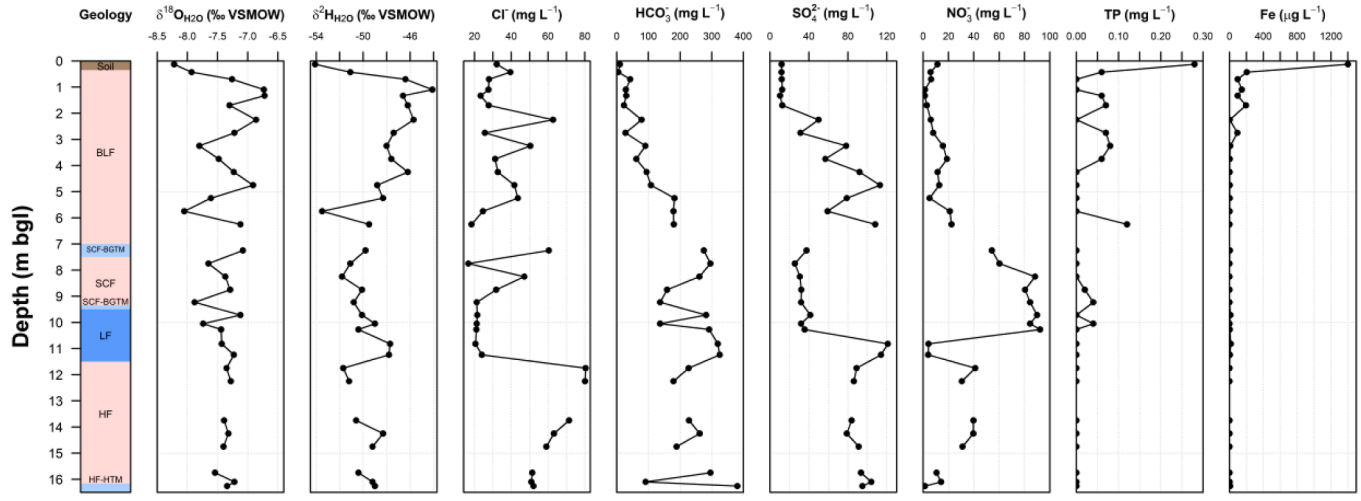

Fig. 5. Vertical stable isotope and hydrochemical profiles for pore waters extracted from glacial deposits at Site F (Park Farm borehole F2). See Fig. 1 for borehole location. Geological nomenclature: BLF, Briton's Lane Formation; SCF, Sheringham Cliffs Formation; BGTM, Bacton Green Till Member; LF, Lowestoft Formation; HF, Happisburgh Formation; HTM, Happisburgh Till Member. Based on Lewis (2014) © Crown copyright and database rights 2014. (For interpretation of the references to colour in this figure legend, the reader is referred to the web version of this article.)

Table 3
Concentrations of CFC and SF_6 residence time indicators for pumped groundwater samples in September 2011, fractions of CFC and SF_6 concentrations in samples relative to modern air-equilibrated water concentrations at 10 °C, and calculated year of recharge.

Sample ID	Concentration			Modern fraction			Year of recharge		
	CFC-12 (pmol/L)	CFC-11 (pmol/L)	SF_6 (fmol L^{-1})	CFC-12	CFC-11	SF_6	CFC-12	CFC-11	SF_6
A1	0.19	0.39	0.00	0.06	0.08	0.00	1960	1963	Pre-1975
A2	0.66	1.01	0.00	0.23	0.20	0.00	1969	1969	Pre-1975
A3	0.37	0.61	0.64	0.13	0.12	0.23	1965	1966	1986
F1	0.18	0.34	0.00	0.06	0.07	0.00	1960	1962	Pre-1975
F2	1.45	3.18	0.59	0.49	0.62	0.21	1977	1978	1985
F3	1.01	1.13	1.00	0.34	0.22	0.36	1973	1969	1990

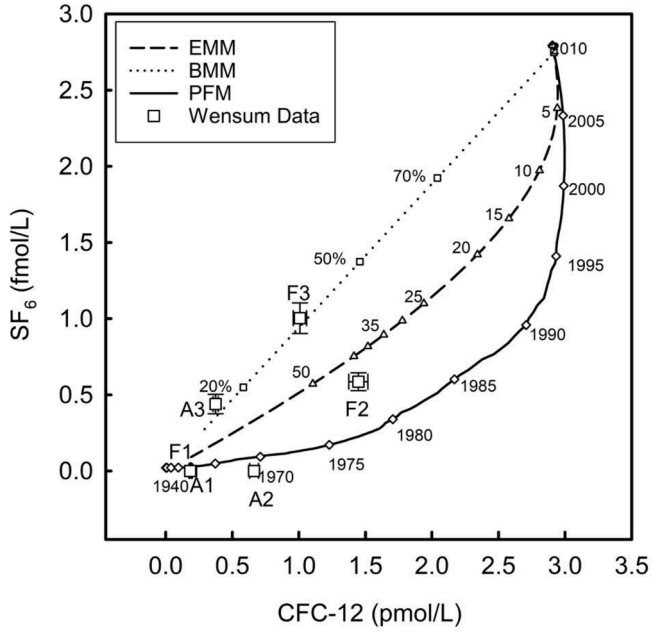

Fig. 6. CFC-12 and SF_6 pumped groundwater concentrations overlaid on the ideal mixing model curves for groundwater at 10 °C. Labelled dates are the groundwater age at that point on the curve. The three mixing models shown include exponential mixing (EMM), binary mixing (BMM) and piston flow (PFM).

(two-sample *t*-test *p* value = 0.001). The less depleted field drainage values are centred on the volume-weighted mean isotopic composition of the spring/summer precipitation ($\delta^{18}O_{H2O} = -6.8$ ‰) at the time of sampling, and the more depleted groundwaters are coincident with the isotopic composition of winter precipitation ($\delta^{18}O_{H2O} = -7.2$ ‰). Field drainage is not present in mini-catchment D and the pumped groundwater samples from Park Farm (Site F) have a narrower compositional range ($\delta^{18}O_{H2O} = -7.5$ to -7.4 ‰) (Fig. 3b) compared with the pumped groundwater samples measured at Site A.

Combining the pumped glacial deposits groundwater data from September 2011 and June 2012 for Site A gives a mean $\delta^{18}O_{H2O}$ value of −7.4 ‰ that is slightly depleted, although not significantly ($p > 0.1$), compared to the mean $\delta^{18}O_{H2O}$ value of −7.2 ‰ for pore waters extracted at this site. For pumped glacial deposits groundwater at Site F, a mean $\delta^{18}O_{H2O}$ value of −7.5 ‰ is slightly depleted, but again not significantly ($p > 0.1$), compared to the mean $\delta^{18}O_{H2O}$ value of −7.4 ‰ for the pore waters at this site.

The five samples from the underlying Chalk aquifer, with a range in $\delta^{18}O_{H2O}$ values of −7.6 to −7.2 ‰, have a similar isotopic composition as the pumped groundwater in the overlying glacial deposits ($\delta^{18}O_{H2O} = -7.9$ to -7.1 ‰). The mean $\delta^{18}O_{H2O}$ values for the Chalk and pumped glacial deposits groundwater are the same at −7.4 ‰ and are not statistically different ($p > 0.1$). Compared with the mean $\delta^{18}O_{H2O}$ value of pore waters in the glacial deposits (−7.3 ‰), the Chalk groundwater is again not statistically different ($p > 0.1$). Together, the evidence supports the conceptual understanding that the superficial glacial deposits and Chalk aquifer are hydraulically connected as an aquifer system (Hiscock, 1993). Overall, the dataset shows that the isotopic

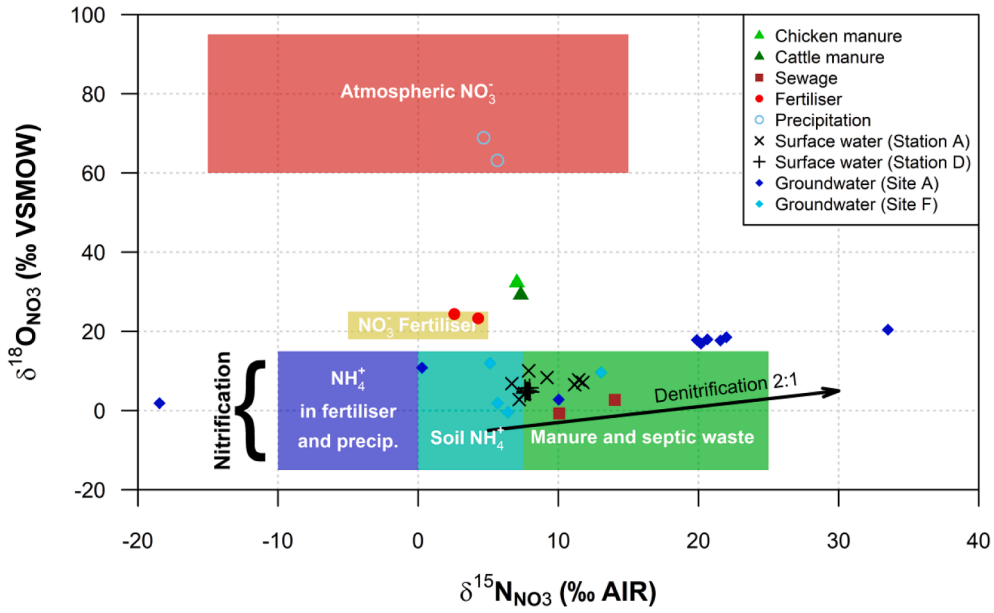

Fig. 7. Values of $\delta^{15}N_{NO3}$ and $\delta^{18}O_{NO3}$ for NO_3^- sources in the River Wensum provided by Wexler (2010) compared with isotopic ranges associated with agricultural sources of NO_3^- adapted from Kendall et al. (2007). A 2:1N:O fractionation ratio representing denitrification is shown with a slope of 0.5. Also included are values for precipitation, pumped groundwater from the glacial deposits and Chalk aquifer at Merrison's Lane (Site A) and Park Farm (Site F), and surface waters from monitoring stations A and D collected in June and September 2012. The cluster of five groundwater samples with mean $\delta^{15}N_{NO3} = +20.9$ ‰ and $\delta^{18}O_{NO3} = +17.8$ ‰ are for borehole A3 measured between 2016 and 17 (Garrard, 2018).

composition of groundwaters in this study compares with a contoured $\delta^{18}O_{H2O}$ value of −7.5 ‰ (±0.5 ‰) for northern East Anglia presented by Darling et al. (2003) for recent (within the Holocene, 0–10 ka) groundwaters of the British Isles.

Pore water samples recovered from the glacial deposits at boreholes A2 and F2 demonstrate a wide range of values ($\delta^{18}O_{H2O} = -8.2$ to −6.6 ‰) that, in the case of Merrison's Lane (Site A), encompass both the field drainage (which is significantly different to the pore waters from borehole A2, $p = 0.001$) and pumped groundwater samples (Fig. 3a). The range of pore water values from boreholes A2 and F2 is similar to that obtained for pore waters in lodgement till in the adjacent River Bure catchment ($\delta^{18}O_{H2O} = -8.1$ to −6.5 ‰; Hiscock et al., 2011). A linear regression of all pore water isotopic values for the Blackwater subcatchment (see Fig. S1 in the SM) yields the relationship $\delta^2H_{H2O} = 4.65\ \delta^{18}O_{H2O} - 14.63$ ($R^2 = 0.50$), consistent with the relationship $\delta^2H_{H2O} = 4.93\ \delta^{18}O_{H2O} - 17.34$ ($R^2 = 0.76$) for pore waters extracted from two cored boreholes in Lowestoft Till at Morley and Cowlinge located, respectively, 35 km and 80 km to the southwest of the current study area in East Anglia (Hiscock and Tabatabai Najafi, 2011).

The pore water stable isotope profile for borehole A2 (Merrison's Lane; Fig. 4) is generally consistent from 4 m bgl, representative of longer-term groundwater recharge. $\delta^{18}O_{H2O}$ values in the range −7.5 to −7.0 ‰ and δ^2H_{H2O} from −49 to −47 ‰ are indicative of recharge under current climatic conditions ($\delta^{18}O_{H2O} = -7.2$ ‰ and $\delta^2H_{H2O} = -48$ ‰; George, 1998) within the silty clay and sand deposits that comprise the Sheringham Cliffs and Lowestoft Formations at this site. Above this depth, stable isotope values in the weathered Bacton Green Till Member are more depleted ($\delta^{18}O_{H2O} < -7.5$ ‰ and $\delta^2H_{H2O} < -50$ ‰) and correspond to the pumped groundwater values ($\delta^{18}O_{H2O} = -7.9$ ‰ and $\delta^2H_{H2O} = -51$ ‰) measured in borehole A4 over a slotted casing interval of 1.0–3.6 m bgl. A similar observation occurs at a depth interval of 11.5–12.0 m bgl within the low-permeability Lowestoft Till Member with stable isotope values of $\delta^{18}O_{H2O} = -7.6$ ‰ and $\delta^2H_{H2O} = -49$ ‰, although this was a poured sample adjacent to the bottom of the overlying glacial sands of the Sheringham Cliffs Formation.

The pore water stable isotope profile for borehole F2 (Park Farm; Fig. 5) yields median values of $\delta^{18}O_{H2O} = -7.3$ ‰ and $\delta^2H_{H2O} = -49$ ‰ (Table 2), again indicative of groundwater recharge under current climatic conditions. The glacial deposits at this location are generally more sand-rich with a higher permeability throughout the profile and show a wide range of stable isotope values. For example, $\delta^{18}O_{H2O}$ ranged from −8.2 ‰ to −6.7 ‰ and δ^2H_{H2O} from −54 ‰ to −44 ‰ from below the soil zone to a depth of 7 m bgl, probably reflecting shorter-term variations in rainfall recharge. Below this depth, more depleted isotope values, for example $\delta^{18}O_{H2O} = -7.9$ ‰ and −7.7 ‰ at depth intervals of 9.1–9.35 m bgl and 10.0–10.1 m bgl, respectively, are recorded in the lower-permeability silty clay deposits of the Bacton Green Till Member and within the Lowestoft Formation and may reflect an older, pre-1950 component of groundwater, similar to that identified by Hiscock et al. (1996) in confined Chalk groundwater from beneath thick glacial till deposits in the adjacent Bure catchment.

3.2. *Groundwater residence time indicators*

The concentration in groundwater of anthropogenic atmospheric trace gases such as chlorofluorocarbons (CFCs) and sulphur hexafluoride (SF_6) can provide information on groundwater residence times and mixing processes for waters up to 70 years old (Cook and Solomon, 1997; Busenberg and Plummer, 2000). The results of the residence time indicator concentrations and apparent groundwater age calculations are shown in Table 3 and a cross-plot of the concentrations for CFC-12 and SF_6 superimposed on the mixing models described in the SM are shown in Fig. 6. The Chalk groundwater samples (A1, F1) and Lowestoft Till Member sample (A2) plot close to the piston flow modelled line (as would be anticipated for a confined aquifer). The shallower samples from boreholes A3 and F3 in the Sheringham Cliffs Formation indicate binary mixing (unconfined) and sample F2 in the lower Happisburgh Formation shows exponential mixing (semi-confined), and so fitting well with the existing hydrogeological conditions.

The residence time indicators suggest a component of modern water throughout the profile of glacial deposits at both Sites A and F with the year of recharge in the underlying Chalk aquifer dating from the early 1960s. From the water level data given in Table 1, downward hydraulic gradients, *i*, of 0.071 and 0.060 existed between the mid-points of the

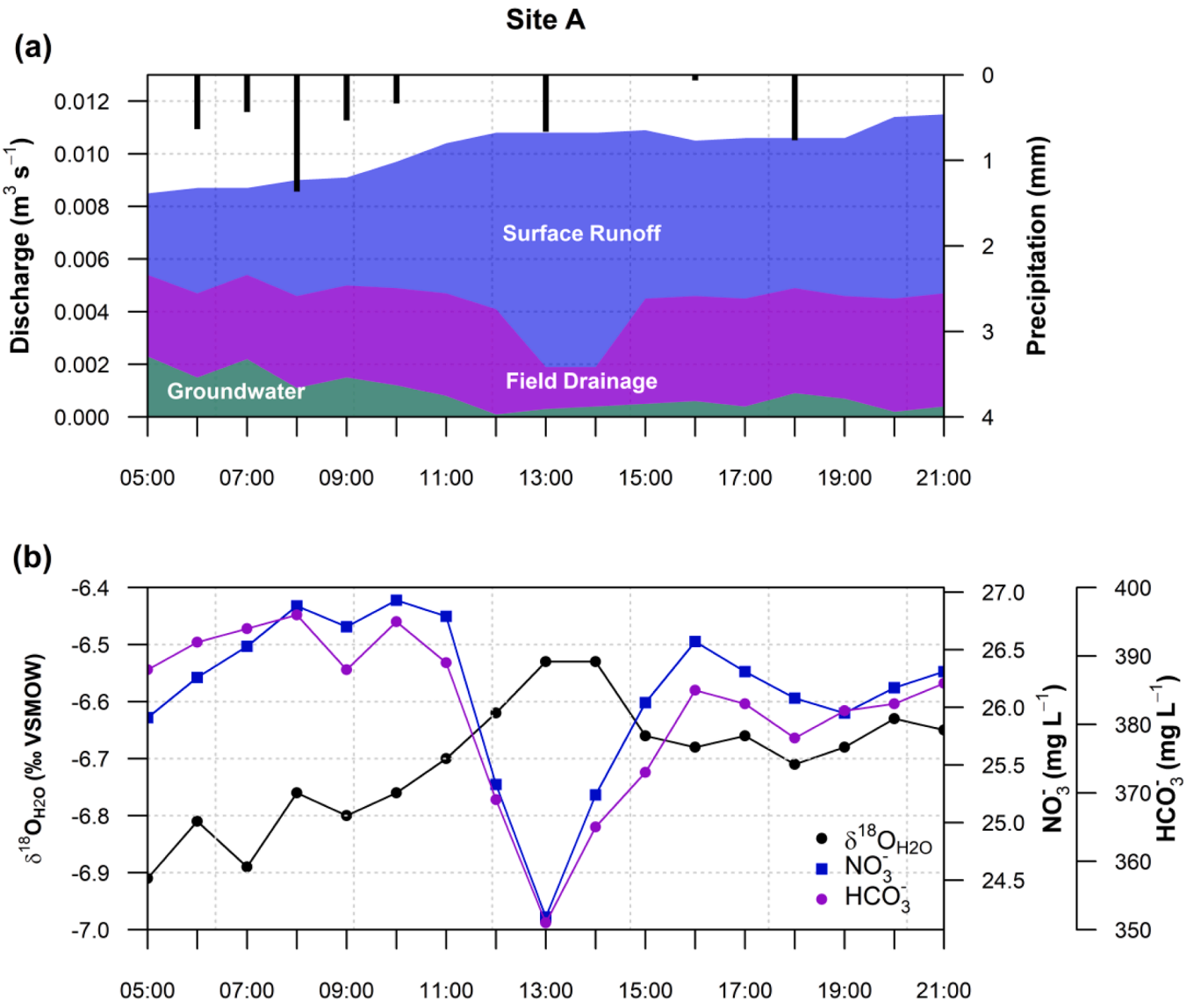

Fig. 8. (a) Mini-catchment A three-component mixing model hydrograph separation for the 17 April 2012 storm event and (b) corresponding stream water stable isotope and hydrochemical data.

slotted casing sections of boreholes A1 and A4 (Merrison's Lane) and F1 and F4 (Park Farm), respectively, in May 2012. From a consideration of Darcy's law applied to the bulk of the till thickness and assuming intergranular flow:

$$\bar{v} = -\frac{iK}{n}$$

then, for a travel time of 50 years through a depth of ~ 15 m of glacial deposits, equal to a percolation rate, $\bar{v}$, of ~ 300 mm a^{-1}, the estimated hydraulic conductivity, K, for the glacial deposits ranges from $2.0 - 2.6 \times 10^{-8}$ m s^{-1} for an estimated porosity, n, of 0.15 (based on the mean saturated moisture content of core material). The hydraulic conductivity values obtained in this study compare with lower values of between 5×10^{-11}–4×10^{-9} m s^{-1} reported at Cowlinge and Morley southwest of the current study area (Hiscock and Tabatabai Najafi, 2011). The difference indicates the greater influence of more sand-rich material within the bulk of the glacial till in the Blackwater sub-catchment compared with locations further south in East Anglia.

3.3. Hydrochemical data

The major ion data shown in Table 2 provide evidence for the influence of agricultural practices and hydrological residence times on the field drainage and groundwater chemistry. Dilute concentrations of Cl^-, NO_3^- and SO_4^{2-} in precipitation, with weighted mean values of 3.2, 0.75 and 2.0 mg L^{-1}, respectively, indicate sources of ions in marine aerosols and the scavenging of nitrogen and sulphur oxides from the atmosphere. In contrast, elevated concentrations of these three parameters in field drainage with mean values of 54.5, 67.9 and 41.8 mg L^{-1}, respectively, represent the infiltration of agricultural contaminants through the soil profile, with NO_3^- and SO_4^{2-} concentrations ranging over two orders of magnitude in response to rainfall flushing events. The influence of rainfall recharge is also apparent in the values of electrical conductivity, which range from 78 to 528 µS cm^{-1} in field drainage with a median value of 444 µS cm^{-1}.

PO_4^{2-} concentrations in field drainage show a wide variation of 2–1051 µg L^{-1} with a median value of 11 µg L^{-1}, with higher concentrations during storm events when phosphorus is mobilised attached to suspended particulate matter (Cooper et al., 2015b). Below the soil zone, PO_4^{2-} concentrations in pumped groundwater (Table 2) and total

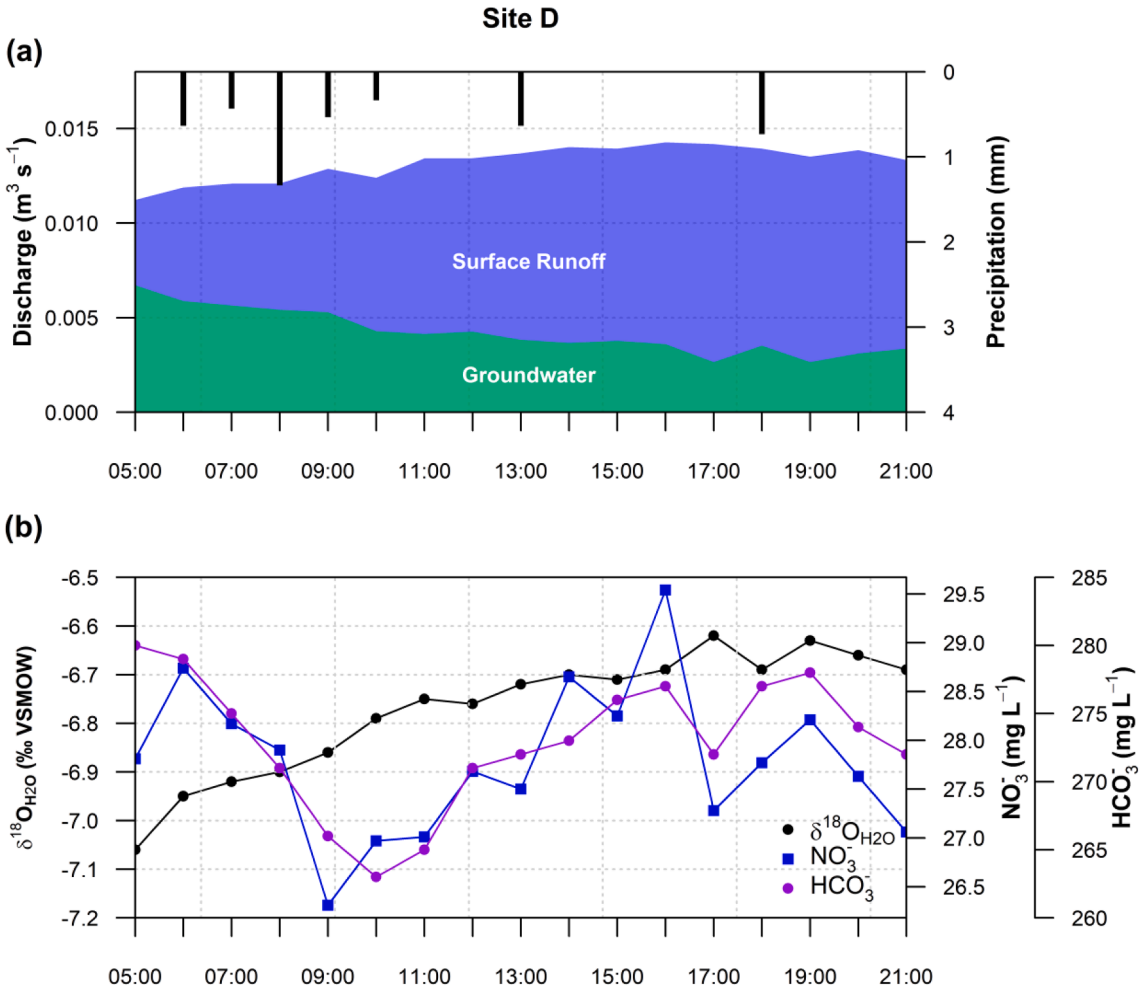

Fig. 9. (a) Mini-catchment D two-component mixing model hydrograph separation for the 17 April 2012 storm event and (b) corresponding stream water stable isotope and hydrochemical data.

phosphorus concentrations in pore waters in the glacial deposits (Figs. 4 and 5) are typically < 100 μg L^{-1}, with higher concentrations associated with the Fe-rich glacial sand deposits, especially in the profile at Park Farm (Site F).

Below the soil profile at Merrison's Lane (Site A), the concentrations of NO_3^- and SO_4^{2-} are strongly influenced by the lithology and mineralogy of the glacial deposits. The pore water samples (Fig. 4) show low concentrations of NO_3^- of < 8 mg L^{-1} throughout the profile but variable SO_4^{2-} concentrations of between 7 and 183 mg L^{-1}. The pore water profiles show a pattern of higher NO_3^- (1–8 mg L^{-1}) and lower SO_4^{2-} (<100 mg L^{-1}) concentrations in the presence of the clay-rich Bacton Green and Lowestoft Till Members from, respectively, 1–5 m bgl and 11–15 m bgl. The opposite occurs at the base of the Bacton Green Till Member and within the underlying glacial sands of the Sheringham Cliffs Formation from 5 to 11 m bgl with NO_3^- concentrations of < 1 mg L^{-1} and SO_4^{2-} from 40 to 140 mg L^{-1}.

The pattern of pore water NO_3^- and SO_4^{2-} concentrations in this study is consistent with the pore water hydrochemistry of glacial deposits in East Anglia presented by Hiscock and Tabatabai Najafi (2011) in which autotrophic denitrification is apparent in the presence of reduced Fe and sulphur species associated with disseminated pyrite in the glacial deposits. Concentrations of total Fe in the range 2–15 μg L^{-1} under chemically reducing conditions developed in the confining glacial till layers and the increase in SO_4^{2-} concentrations due to pyrite oxidation to concentrations above those observed in agricultural drainage (~40 mg L^{-1}) further support this interpretation. NO_3^- and SO_4^{2-} concentrations of < 1.3 mg L^{-1} and ~ 45 mg L^{-1}, respectively, in pumped groundwater samples from the glacial deposits at Merrison's Lane (Table 2) also demonstrate the importance of the slow recharge rate and opportunity for denitrification in the clay-rich glacial tills overlying the Chalk aquifer at this site.

Additional denitrification may be promoted by the presence of organic matter in the glacial deposits, with an associated increase in HCO_3^-, although the higher HCO_3^- concentrations of 180–450 mg L^{-1} in the chalk-rich glacial tills (Fig. 4) are primarily due to weathering and the incongruent dissolution of carbonate (Hiscock, 1993). It is possible that denitrification involving a multiple electron donor system develops, for example where organic carbon, sulphide and Fe minerals are all available (Rivett et al., 2008), as identified by Postma et al. (1991) for an unconfined sandy aquifer of Quaternary age in Jutland, Denmark.

The presence of NO_3^- in the Merrison's Lane pore water profile below 11 m bgl (Fig. 4) shows that agricultural contaminants can penetrate the low-permeability, clay-rich glacial deposits at this site, consistent with groundwater residence times of several decades (Table 3) corresponding with the era of increased fertiliser applications. The clay-rich deposits can exhibit slow, diffusion dominated water and solute transport (Hiscock et al., 2011) except, as in the Blackwater sub-catchment, where intercalated sand and gravel-rich layers within the glacial till provide pathways along which relatively modern groundwater can move. Evidence for oxygenated groundwater flow along sub-horizontal fractures within glacial till is occasionally observed where orange staining from Fe oxidation is present (for example, see left-hand core section

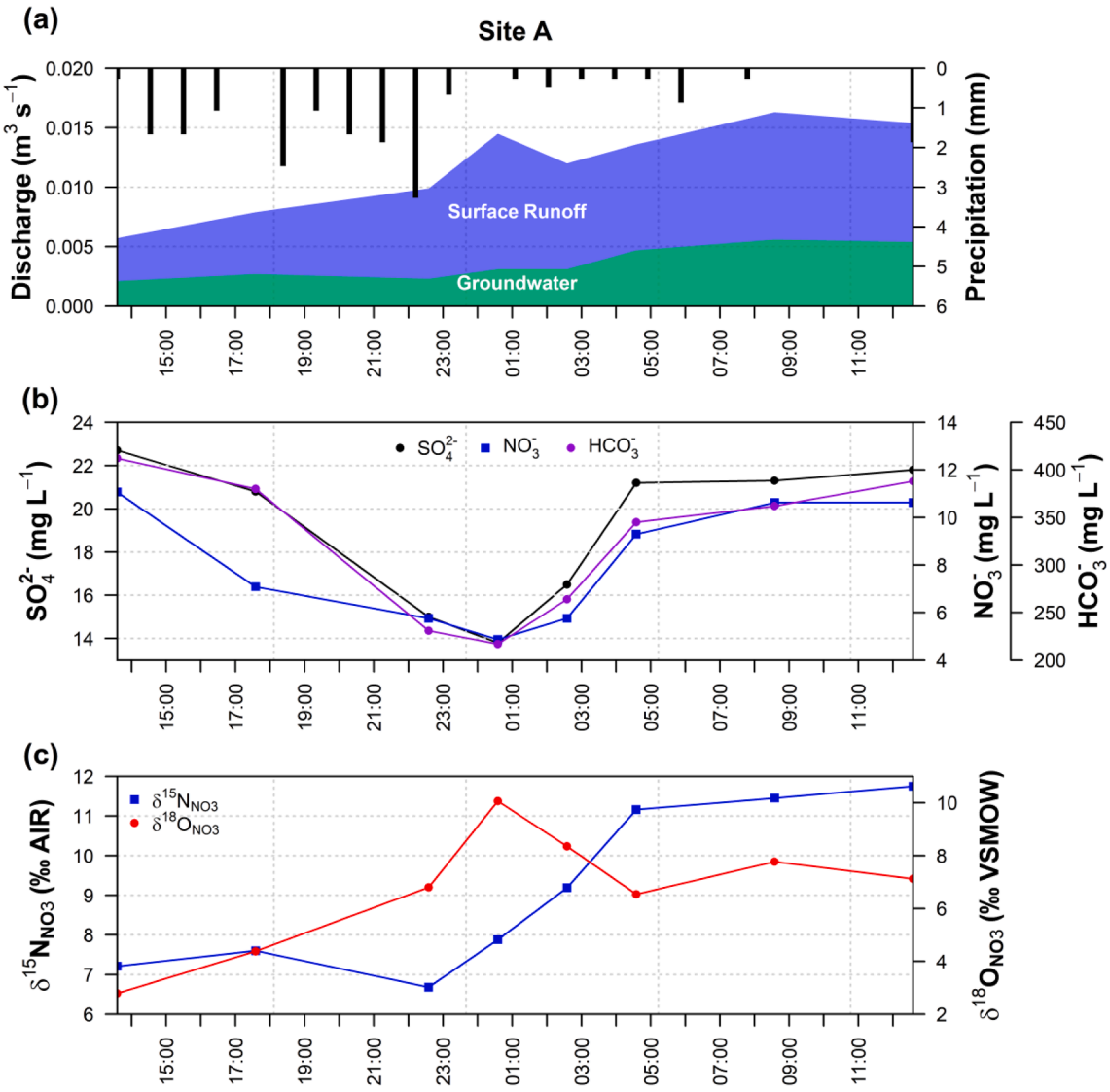

Fig. 10. (a) Mini-catchment A two-component mixing model hydrograph separation for the 23–24 September 2012 storm event and corresponding (b) hydrochemical and (c) dual stable isotopes of NO_3^- data.

photograph in the Graphical Abstract of the Bacton Green Till Member (5.5–6.0 m bgl) in borehole A2).

At Park Farm (Site F), pumped groundwater samples in the glacial deposits recorded NO_3^- and SO_4^{2-} concentrations in the ranges 30.9–65.2 mg L^{-1} and 26.1–91.7 mg L^{-1}, respectively. The higher permeability of the glacial deposits is evident in the pore water profiles for Park Farm (Fig. 5) where there is only limited evidence for denitrification, for example the low NO_3^- (3.9–4.2 mg L^{-1}) and higher SO_4^{2-} (114–121 mg L^{-1}) concentrations between 10.5 and 11.5 m bgl associated with the lower permeability Lowestoft Formation. Mean NO_3^- concentrations in pore water (Table 2) are an order of magnitude higher at Park Farm (30.3 mg L^{-1}) compared with Merrison's Lane (2.41 mg L^{-1}), with particularly elevated concentrations of 54–92 mg L^{-1} at a depth of 7.0–10.3 m bgl in glacial sands of the Sheringham Cliffs Formation and into the upper part of the underlying Lowestoft Formation. Lower NO_3^- concentrations of < 40 mg L^{-1} are more typical throughout the remainder of the profile.

The presence of agricultural NO_3^- in the pumped groundwater and pore water samples at Park Farm and the absence of significant denitrification indicates a shorter groundwater residence time and the existence of oxidising conditions in the glacial deposits. Additional evidence for oxidising conditions are the low total Fe concentrations (<14 μg L^{-1} at depths greater than 3 m bgl) that suggest that Fe exists as $Fe(OH)_3$. The influence of lithology is further apparent with pore water HCO_3^- values in the range 137–296 mg L^{-1} in the sands and gravels of the deeper Briton's Lane, Sheringham Cliffs and Happisburgh Formations. The lowest HCO_3^- concentrations (<108 mg L^{-1}) are observed in a weathered zone from the ground surface to a depth of 5 m bgl (Fig. 5) in the carbonate-deficient glacial sand and gravel of the Briton's Lane Formation.

3.4. Nitrate stable isotope data

Fig. 7 shows the isotopic composition of typical sources of NO_3^- for the agricultural system in the Wensum catchment including inorganic and organic fertilisers and local municipal (sewage) waste from data presented by Wexler (2010). Also shown are the isotopic composition of precipitation collected on 18 September 2012, pumped groundwater samples from the Merrison's Lane (Site A) and Park Farm (Site F) boreholes collected on 18 June 2012 and stream water samples collected during a storm event captured on 23–24 September 2012 at monitoring stations A and D. An additional five pumped groundwater samples were

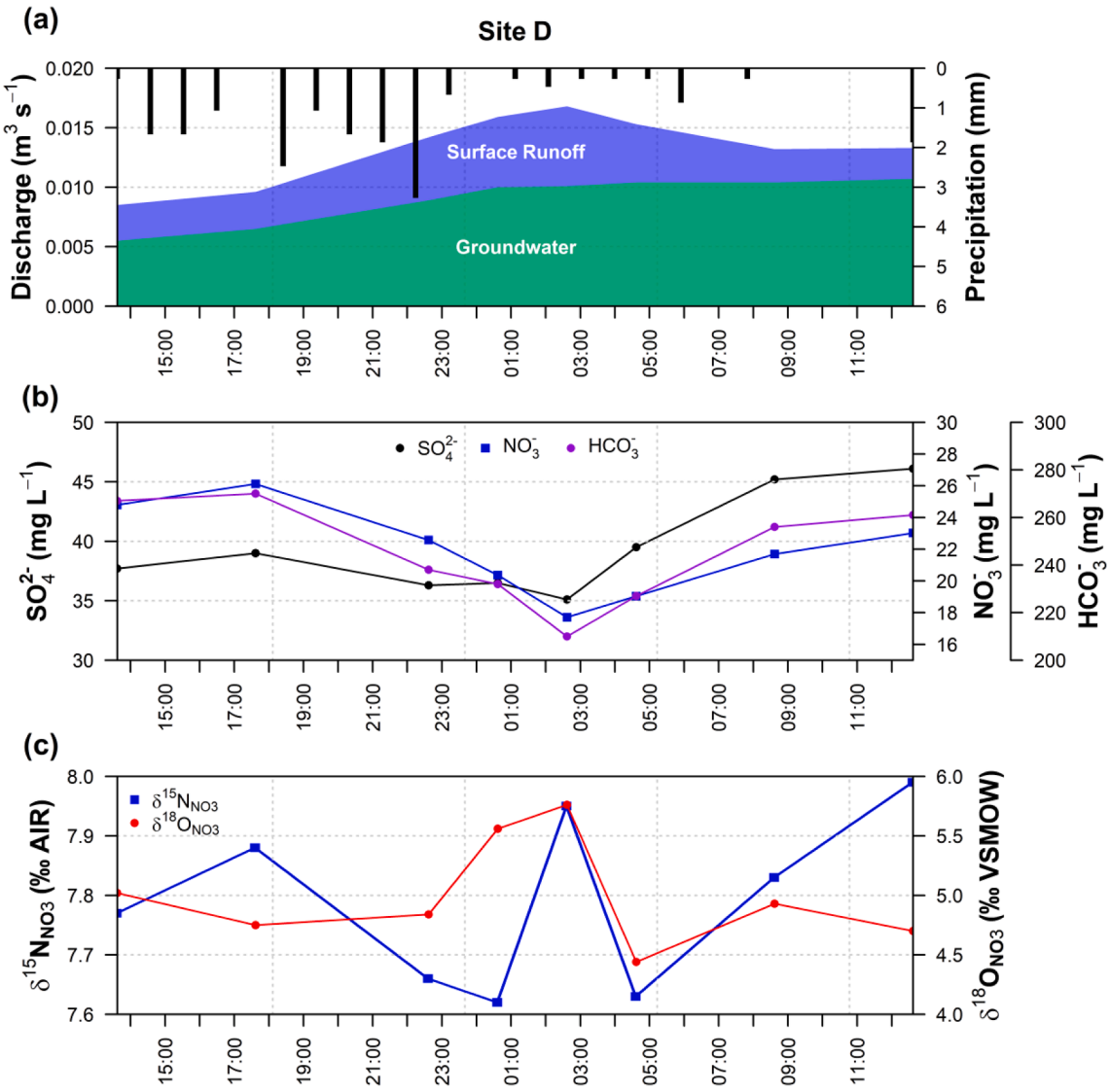

Fig. 11. (a) Mini-catchment D two-component mixing model hydrograph separation for the 23–24 September 2012 storm event and corresponding (b) hydrochemical and (c) dual stable isotopes of NO_3^- data.

collected for dual stable isotope analysis from borehole A3 (slotted casing interval 5.0–12.0 m bgl) at Merrison's Lane between 2016 and 2017 by Garrard (2018).

The NO_3^- isotopic composition of all stream water samples reflected a mix of influences, as expected during a dynamic storm event when microbially cycled NO_3^- in the soil profile is mixed with NO_3^- from precipitation and sources flushed from the soil. The $\delta^{18}O_{NO3}$ values of stream water samples suggest NO_3^- produced from nitrification of NH_4^+ ($\delta^{18}O_{NO3} = +2.8$ to $+3.8$ ‰), with most samples also carrying a signal from isotopic fractionation due to denitrification resulting in higher values in both $\delta^{15}N_{NO3}$ and $\delta^{18}O_{NO3}$. This pattern may be the result of a mixing of NO_3^- from nitrification with partially denitrified NO_3^-, or could indicate that nitrification was followed by partial denitrification. In addition, some samples had elevated $\delta^{18}O_{NO3}$ values without elevated $\delta^{15}N_{NO3}$ values indicating mixing of NO_3^- from precipitation ($\delta^{18}O_{NO3} = +63.2$ and 68.9 ‰) or chemical fertiliser NO_3^- ($\delta^{18}O_{NO3} = +23.2$ and 24.4 ‰). Higher $\delta^{15}N_{NO3}$ values in stream water in the range $+9$ to $+12$ ‰ may also indicate nitrogen from manure and septic wastes, although not a significant nitrogen source in the study area.

Most groundwater samples had $\delta^{15}N_{NO3}$ and $\delta^{18}O_{NO3}$ values close to those of the stream water samples but with a larger range, such that the range of stream water isotopic composition is encompassed within the range of groundwater isotopic composition (Fig. 7). One groundwater sample (borehole A3) showed a pronounced effect of denitrification in a high level of isotopic fractionation ($\delta^{15}N_{NO3} = +33.5$ ‰, $\delta^{18}O_{NO3} = +20.5$ ‰), with repeat sampling between 2016 and 2017 (Garrard, 2018) (Fig. 7) giving mean values of $\delta^{15}N_{NO3} = +20.9$ ‰ and $\delta^{18}O_{NO3} = +17.8$ ‰. This borehole was pumped over a slotted casing interval of 5.0——12.0 m bgl in the glacial sands of the Sheringham Cliffs Formation (Table 1) and the isotopic values are consistent with the hydrochemical evidence for denitrification within the glacial sands at this horizon observed in the pore water profile (Fig. 4). The groundwater and stream water samples recorded $\delta^{18}O_{NO3}$ values of between -0.4 ‰ to $+12.0$ ‰ below the range reported for inorganic nitrogen fertiliser ($+15$ to $+25$ ‰) (Kendall, 1998).

3.5. Storm hydrograph response

Further insight into the influence of the glacial deposits on hydrological and NO_3^- transport processes in the Blackwater sub-catchment was explored in mini-catchments A and D for two contrasting storm events on 17 April and 23–24 September 2012. Antecedent catchment conditions in the seven months prior to April 2012 were drier than normal with only 71 % of the long-term average (1971–2000)

Table 4
Mixing model end-member components and parameter values applied to storm hydrograph separation of the 17 April and 23–24 September 2012 events in mini-catchments A (chalky tills and silty clays) and D (glacial sands and gravels).

Component	Mini-catchment A (17 April)		Mini-catchment D (17 April)	Mini-catchment A (23–24 Sept)	Mini-catchment D (23–24 Sept)
	$\delta^{18}O_{H2O}$ (‰ VSMOW)	NO_3^- (mg L^{-1})	$\delta^{18}O_{H2O}$ (‰ VSMOW)	SO_4^{2-} (mg L^{-1})	SO_4^{2-} (mg L^{-1})
Surface runoff (event)	−6.42[a]	0.75[d]	−6.42[a]	2.01[h]	2.01[h]
Subsurface field drainage	−6.93[b]	67.9[e]	–	–	–
Groundwater (pre-event)	−7.56[c]	4.18[f]	−7.35[g]	58.0[i]	56.9[j]

[a] Mean of two precipitation samples collected 16–17/04/12.
[b] Median of field drain samples collected 30/04/12–01/05/12 (Table 2).
[c] Median of pore water samples from 0 to 4.8 m bgl in Merrison's Lane (Site A) borehole A2.
[d] Weighted mean of precipitation samples collected 03/04/12–16/06/12 (Table 2).
[e] Mean of field drain samples collected 30/04/12–01/05/12 (Table 2) except for sample times 13:00 and 14:00 h on 17/04/12 when modelled NO_3^- concentrations were 164 and 171 mg L^{-1}, respectively, were required to reach a solution with a positive contribution from the groundwater fraction.
[f] Median of pore water samples from 0.3 to 4.8 m bgl in Merrison's Lane (Site A) borehole A2.
[g] Median of pore water samples from 0 to 16.0 m bgl in Park Farm (Site F) borehole F2.
[h] Weighted mean of precipitation samples collected 03/04/12–16/06/12.
[i] Median of pore water samples from 0 to 14.3 m bgl in Merrison's Lane (Site A) borehole A2.
[j] Median of pore water samples from 0 to 16.3 m bgl in Park Farm (Site F) borehole F2.

precipitation while the four months prior to September 2012 were wetter than normal with 154 % of the long-term average.

The storm event monitored on 17 April started at 05:00 h and lasted 17 h. Precipitation measured at rain gauges in each of the mini-catchments A and D (RG1 and RG5, respectively) occurred in a main pulse of 3 mm in the first five hours of the storm and then further, smaller pulses in the next eight hours to give a precipitation total of 4.2 mm at the end of the event (Fig. 8a and 9a). The second storm event from 23 to 24 September started at 13:00 h and lasted 25 h. Compared with the April event, a greater precipitation total of 15.0 mm (RG1, mini-catchment A) and 17.8 mm (RG5, mini-catchment D) fell in the first 11 h of the storm followed by smaller totals of 4.0 mm and 3.2 mm, respectively, in the remaining 14 h (Fig. 10a and 11a).

At monitoring station A, total discharge increased 33 % during the April storm event from 0.009 m^3/s at 05:00 h to 0.012 m^3/s at 21:00 h (Fig. 8a). At monitoring station D, total discharge also increased but by only 8 % from 0.012 m^3/s at 05:00 h to 0.013 m^3/s at 21:00 h, having reached a peak discharge of 0.014 m^3/s at 16:00 h (Fig. 9a). During the September storm event, the greater precipitation amount gave a more pronounced increase in stream discharge. At monitoring station A, total discharge increased 150 % during the event from 0.006 m^3/s at 13:00 h on 23 September to 0.015 m^3/s at 13:00 h on 24 September, with a peak discharge of 0.016 m^3/s at 09:00 h on 24 September (Fig. 10a). At monitoring station D, total discharge increased by a smaller 44 % from 0.009 m^3/s at 13:00 h on 23 September to 0.013 m^3/s at 13:00 h on 24 September, with a peak discharge of 0.017 m^3/s at 02:00 h on 24 September (Fig. 11a).

For the April event, three- and two-component mixing models were applied to mini-catchments A and D, respectively, with values of $\delta^{18}O_{H2O}$ and NO_3^- selected for the end-member components given in Table 4. The hydrograph separation for mini-catchment A showed that before the onset of precipitation, field drainage and groundwater generated 36 % and 27 % of the total discharge, respectively (Fig. 8a). By 13:00 h, five hours after the mid-point of the first pulse of precipitation, the stream water NO_3^- and HCO_3^- decreased from initial concentrations of 25.9 mg L^{-1} and 388 mg L^{-1} to their lowest values of 24.2 mg L^{-1} and 351 mg L^{-1}, respectively, resulting from dilution with surface runoff (event water) (Fig. 8b). At this time, field drainage and groundwater accounted for 14 % and 3 % of the total discharge, respectively. Thereafter, and with two further pulses of 1 mm of precipitation at 13:00 and 18:00 h, the contributions of field drainage and groundwater to the total discharge were on average 38 % and 5 %, respectively, highlighting the importance of surface runoff and subsurface field drainage in mini-catchment A with its low permeability clay loam substrate.

The response of mini-catchment D to the April storm event showed that the contribution of groundwater to the total stream discharge was 69 % at the start of the storm, then decreased to a minimum of 22 % at 17:00 h, before increasing by a small amount to 29 % by the end of the storm at 21:00 h (Fig. 9a). Minimum concentrations of NO_3^- and HCO_3^- of 26.3 mg L^{-1} and 263 mg L^{-1}, respectively, were observed 3–4 h after the onset of the storm (Fig. 9b), recovering to higher concentrations of 29.5 mg L^{-1} at 16:00 h and 278 mg L^{-1} at 19:00 h, respectively, towards the end of the storm. Hence, compared to mini-catchment A, the more permeable sandy clay loam substrate that underlies mini-catchment D supported a higher groundwater component of stream discharge throughout the storm event that was characterised by a similar range in NO_3^- but with a lower range in HCO_3^- concentrations.

For the September event, a two-component mixing model was applied to both mini-catchments A and D with values of SO_4^{2-} chosen for the end-member components given in Table 4. The hydrological response to precipitation showed an increased contribution of groundwater to the total stream discharge with minimum values of 21 % and 60 % recorded 11 and 13 h after the start of the storm in mini-catchments A and D, respectively, with the quicker response observed in mini-catchment A with its underlying lower permeability clay loam substrate (Fig. 10a and 11a). At the end of the storm, the groundwater contribution in mini-catchment A (35 %) was similar to that at the start (37 %). In mini-catchment D, the groundwater contribution increased from 65 % at the start of the storm to 80 % at the end and again highlights the importance of the more permeable sandy clay loam substrate in maintaining baseflow in this mini-catchment.

The hydrochemical response to the September storm event demonstrated that the lowest concentrations of NO_3^- and HCO_3^- in mini-catchments A and D occurred 1.5 and 3.5 h, respectively, after the end of the main period of precipitation (Fig. 10b and 11b). The response is similar to the storm event in April in that the more clay-rich mini-catchment A responded faster than the more sand-rich and baseflow-controlled mini-catchment D.

The pulse of surface runoff in the September storm event is also apparent in the $\delta^{18}O_{NO3}$ signatures, with more enriched values of + 10.1 ‰ and + 5.8 ‰ in mini-catchments A and D, respectively, reflecting a contribution of NO_3^- from atmospheric nitrogen in precipitation (Fig. 10c and 11c). Thereafter, NO_3^- and HCO_3^- concentrations recovered to values similar to those recorded at the start of the storm, with NO_3^- concentrations recorded in mini-catchments A and D of 10.7 mg L^{-1} and

22.8 mg L^{-1}, respectively, by the end of the storm. During the second half of the storm when stream discharge continued to rise in mini-catchment A, $\delta^{15}N_{NO3}$ values increased from + 7.9 ‰ at 00:30 h to + 11.8 ‰ at 12:30 h, indicative of a denitrified source of nitrogen in groundwater contributing increasingly to the stream water NO_3^-. This observation supports evidence presented by Wexler et al. (2011) and Garrard et al. (2023) who estimated between 15 and 30 % and 30–73 % of leached soil nitrogen is removed by denitrification in groundwater discharging, respectively, to the main river channel and tributary headwaters of the Wensum. $\delta^{15}N_{NO3}$ signatures in mini-catchment D are more tightly constrained in the range + 7.6 ‰ and + 8.0 ‰ (mean = +7.8 ‰) throughout the storm and reflect the importance of baseflow with a soil NO_3^- source influenced by nitrification in the glacial sands and gravels that underlie this mini-catchment.

4. Conclusions

In this study, the presence of low-permeability glacial tills of the Sheringham Cliffs and Lowestoft Formations limits the penetration of agricultural NO_3^- whereas in areas with predominantly higher-permeability glacial sands and gravels of the Briton's Lane, Sheringham Cliffs and Happisburgh Formations, NO_3^- can penetrate the glacial deposits relatively easily. Pore water stable isotope profiles revealed slightly more depleted values ($\delta^{18}O_{H2O} < -7.5$ ‰ and $\delta^{2}H_{H2O} < -50$ ‰) within the low-permeability glacial tills compared with the higher permeability glacial sands and gravels (median values $\delta^{18}O_{H2O} = -7.3$ ‰ and $\delta^{2}H_{H2O} = -49$ ‰). The residence time indicators suggested a component of modern water throughout the profile of the glacial deposits, with the year of recharge in the underlying Chalk aquifer dating from the early 1960 s. The presence of pyrite within the clay-rich glacial deposits means that any NO_3^- in modern recharge is attenuated by denitrification in contrast to the shorter residence time and oxidising conditions that limit any significant denitrification in the glacial sands and gravels.

The influence of the glacial deposits is also evident in the catchment response to storm events with areas underlain by clay loam soils experiencing a faster response to precipitation inputs with a lower baseflow contribution in contrast to the dampened response to precipitation and a higher baseflow component in areas with predominantly sandy clay loam soils. The sources and processes controlling NO_3^- in stream discharge during a storm event also showed the influence of lithology with NO_3^- stable isotope evidence of a denitrified source in baseflow ($\delta^{15}N_{NO3}$ in the range + 6.7 to + 11.8 ‰) contributing to stream flow in areas underlain by glacial tills and a soil NO_3^- source influenced by nitrification in baseflow ($\delta^{15}N_{NO3}$ in the range + 7.6 to + 8.0 ‰) in areas underlain by glacial sands and gravels.

In conclusion, this study demonstrates that the sediment heterogeneity of Pleistocene glacial deposits affects both hydrogeological and geochemical conditions, which then influences contaminant fate. Hence, the glacial geological setting must be considered when evaluating and implementing catchment management practices, as some areas will be better suited to mitigate the impact of agricultural NO_3^- (Best et al., 2015). For example, mitigation measures in arable systems such as improved nutrient management plans and better timing of fertiliser applications to avoid surface and shallow subsurface runoff on soils developed on glacial tills are recommended. For soils developed on glacial sand and gravels with limited denitrification potential, the growing of autumn cover crops to reduce post-harvest nutrient losses in groundwater recharge and the growing of crops with less fertiliser requirements are recommended (Cooper et al., 2017, 2020).

CRediT authorship contribution statement

Kevin M. Hiscock: Conceptualization, Formal analysis, Funding acquisition, Investigation, Methodology, Writing – original draft. **Richard J. Cooper:** Data curation, Formal analysis, Investigation, Methodology, Writing – review & editing. **Melinda A. Lewis:** Data curation, Formal analysis, Funding acquisition, Investigation, Methodology, Writing – review & editing. **Daren C. Gooddy:** Data curation, Formal analysis, Funding acquisition, Investigation, Methodology, Writing – review & editing. **Thomas J. Howson:** Data curation, Investigation, Methodology, Writing – review & editing. **Sarah K. Wexler:** Data curation, Investigation, Methodology, Writing – review & editing.

Declaration of competing interest

The authors declare the following financial interests/personal relationships which may be considered as potential competing interests: Kevin Hiscock reports financial support was provided by the United Kingdom Department for Environment, Food and Rural Affairs.

Data availability

Data will be made available on request.

Acknowledgements

This research was supported by the River Wensum Demonstration Test Catchment project funded by the Department for Environment, Food and Rural Affairs (Defra) (awards WQ0212 and LM0304). Additional funding for the pore water sampling and analysis was provided by BGS through its Groundwater Science Programme. We are grateful to Salle Farms Co. for hosting monitoring equipment and granting access. Anglian Water kindly provided sampling access to Salle Pumping Station. We thank Simon Ellis, Jenny Stevenson and John Brindle for fieldwork support and Alina Marca, Liz Rix, Alina Mihailova, Kim Goodey, Tony Hinchliffe, Graham Chilvers and Andy Hind for laboratory support. The following BGS staff are thanked for their contributions to the project: Michael Bird, Ian Woods, James Sorensen, Peter Williams, Dave Entwisle and David Morgan for assistance with borehole drilling supervision, geological logging and core material processing. Steve Booth and Jonathan Lee assisted with the geological interpretation. Daren Gooddy and Melinda Lewis publish with the permission of the Executive Director, British Geological Survey (UKRI).

Appendix A. Supplementary data

Supplementary data to this article can be found online at https://doi.org/10.1016/j.jhydrol.2024.130982.

References

Best, A., Arnaud, E., Parker, B., Aravena, R., Dunfield, K., 2015. Effects of glacial sediment type and land use on nitrate patterns in groundwater. Groundwater Monitoring & Remediation 35, 68–81.

Bradley, P.M., Kolpin, D.W., Thompson, D.A., Romanok, K.M., Smalling, K.L., Breitmeyer, S.E., Cardon, M.C., Cwiertny, D.M., Evans, N., Field, R.W., Focazio, M.J., Beane Freeman, L.E., Givens, C.E., Gray, J.L., Hager, G.L., Hladik, M.L., Hofmann, J. N., Jones, R.R., Kanagy, L.K., Lane, R.F., Blaine McCleskey, R., Medgyesi, D., Medlock-Kakaley, E.K., Meppelink, S.M., Meyer, M.T., Stavreva, D.A., Ward, M.H., 2023. Juxtaposition of intensive agriculture, vulnerable aquifers, and mixed chemical/microbial exposures in private-well tapwater in Northeast Iowa. Sci. Total Environ. 868, 161672 https://doi.org/10.1016/j.scitotenv.2023.161672.

Burri, N.M., Weatherl, R., Moeck, C., Schirmer, M., 2019. A review of threats to groundwater quality in the anthropocene. Sci. Total Environ. 684, 136–154.

Busenberg, E., Plummer, L.N., 2000. Dating young groundwater with sulphur hexafluoride: Natural and anthropogenic sources of sulfur hexafluoride. Water Resour. Res. 36, 3011–3030.

Casciotti, K.L., Sigman, D.M., Hastings, M.G., Böhlke, J.K., Hilkert, A., 2002. Measurement of the oxygen isotopic composition of nitrate in seawater and freshwater using the denitrifier method. Anal. Chem. 74, 4905–4912.

Cook, P.G., Solomon, D.K., 1997. Recent advances in dating young groundwater: chlorofluorocarbons, $^{3}H/^{3}He$ and ^{85}Kr. J. Hydrol. 191, 245–265.

Cooper, R.J., Hiscock, K.M., 2023. Two decades of the EU water framework directive: evidence of successes and failures from a lowland arable catchment (River Wensum, UK). Sci. Total Environ. 869, 161837 https://doi.org/10.1016/j.scitotenv.2023.161837.

Cooper, R.J., Krueger, T., Hiscock, K.M., Rawlins, B.G., 2015a. High-temporal resolution fluvial sediment source fingerprinting with uncertainty: a Bayesian approach. Earth Surf. Proc. Land. 40, 78–92.
Cooper, R.J., Rawlins, B.G., Krueger, T., Lézé, B., Hiscock, K.M., Pedentchouk, N., 2015b. Contrasting controls on the phosphorus concentration of suspended particulate matter under baseflow and storm event conditions in agricultural headwater streams. Sci. Total Environ. 533, 49–59.
Cooper, R.J., Hama-Aziz, Z., Hiscock, K.M., Lovett, A.A., Dugdale, S.J., Sünnenberg, G., Noble, L., Beamish, J., Hovesen, P., 2017. Assessing the farm-scale impacts of cover crops and non-inversion tillage regimes on nutrient losses from an arable catchment. Agr. Ecosyst. Environ 237, 181–193.
Cooper, R.J., Hiscock, K.M., Lovett, A.A., Dugdale, S.J., Sünnenberg, G., Garrard, N.L., Outram, F.N., Hama-Aziz, Z.Q., Noble, L., Lewis, M.A., 2018. Application of high-resolution telemetered sensor technology to develop conceptual models of catchment hydrogeological processes. J. Hydrol. X 1, 100007. https://doi.org/10.1016/j.hydroa.2018.100007.
Cooper, R.J., Hama-Aziz, Z.Q., Hiscock, K.M., Lovett, A.A., Vrain, E., Dugdale, S.J., Sünnenberg, G., Dockerty, T., Hovesen, P., Noble, L., 2020. Conservation tillage and soil health: lessons from a 5-year UK farm trial (2013–2018). Soil Tillage Res. 202, 104648 https://doi.org/10.1016/j.still.2020.104648.
Craig, H., 1961. Isotopic variations in meteoric water. Science 133, 1702–1703.
Cui, R., Zhang, D., Wang, H., Fu, B., Yan, H., Hu, W., Liu, G., Chen, A., 2023. Shifts in the sources and fates of nitrate in shallow groundwater caused by agricultural intensification: revealed by hydrochemistry, stable isotopic composition and source contribution. Agr Ecosyst Environ 345, 108337. https://doi.org/10.1016/j.agee.2022.108337.
Cuthbert, M.O., Mackay, R., Tellam, J.H., Thatcher, K.E., 2010. Combining unsaturated and saturated hydraulic observations to understand and estimate groundwater recharge through glacial till. J. Hydrol. 391, 263–276.
Darling, W.G., Bath, A.H., Talbot, J.C., 2003. The O & H stable isotopic composition of fresh waters in the British Isles. 2. surface waters and groundwater. Hydrol. Earth Syst. Sci. 7, 183–195.
Durand, P., Neal, M., Neal, C., 1993. Variations in stable oxygen isotope and solute concentrations in small submediterranean montane streams. J. Hydrol. 144, 283–290.
Ferris, D.M., Potter, G., Ferguson, G., 2020. Characterization of the hydraulic conductivity of glacial till aquitards. Hydrgeol. J. 28, 1827–1839.
Fleckenstein, J.H., Niswonger, R.G., Fogg, G.E., 2006. River-aquifer interactions, geologic heterogeneity, and low-flow management. Ground Water 44, 837–852.
Gao, Y., Cabrera Serrenho, A., 2023. Greenhouse gas emissions from nitrogen fertilizers could be reduced by up to one-fifth of current levels by 2050 with combined interventions. Nature Food 4, 170–178.
Garcia-Hernandez, J.A., Brouwer, R., Pinto, R., 2022. Estimating the total economic costs of nutrient emission reduction policies to halt eutrophication in the Great Lakes. e2021WR030772 Water Resour. Res. 58. https://doi.org/10.1029/2021WR030772.
Garrard, N.L., Hiscock, K.M., Cooper, R.J., Marca, A.D., Sünnenberg, G., 2023. Hydrochemical and dual-isotope approach to the identification of denitrification in arable field drainage in the Wensum catchment, eastern England. Appl. Geochem. 158, 105803 https://doi.org/10.1016/j.apgeochem.2023.105803.
Garrard, N.L., 2018. *A stable isotope and hydrochemical approach to examining denitrification along a shallow groundwater–surface water continuum in an agriculturally-impacted catchment.* PhD thesis, University of East Anglia, Norwich, UK, 268 pp.
George, M.A., 1998. High precision stable isotope imaging of groundwater flow dynamics in the Chalk aquifer systems of Cambridgeshire and Norfolk. PhD thesis. University of East Anglia, Norwich, UK, pp. 164–165.
Gooddy, D.C., Darling, W.G., Abesser, C., Lapworth, D.J., 2006. Using chlorofluorocarbons (CFCs) and Sulphur hexafluoride (SF6) to characterise groundwater movement and residence time in a lowland Chalk catchment. J. Hydrol. 330, 44–52.
Gospodyn, L., Wellen, C., Sorichetti, R.J., Mundle, S.O.C., 2023. Using stable water isotopes to evaluate water flow and nonpoint source pollutant contributions in three southern Ontario agricultural headwater streams. Hydrol. Process. 37, e14802.
Gros, M., Catalán, N., Mas-Pla, J., Čelić, M., Petrović, M., Farré, M.J., 2021. Groundwater antibiotic pollution and its relationship with dissolved organic matter: identification and environmental implications. Environ. Pollut. 289, 117927 https://doi.org/10.1016/j.envpol.2021.117927.
Hama-Aziz, Z.Q., Hiscock, K.M., Cooper, R.J., 2017. Dissolved nitrous oxide (N_2O) dynamics in agricultural field drains and headwater streams in an intensive arable catchment. Hydrol. Process. 31, 1371–1381.
Hendry, M.J., Barbour, S.L., Schmeling, E.E., 2016. Defining near-surface groundwater flow regimes in the semi-arid glaciated plains of North America. Isot. Environ. Health Stud. 52, 203–213.
Hiscock, K.M., 1993. The influence of pre-Devensian glacial deposits on the hydrogeochemistry of the Chalk aquifer system of North Norfolk, UK. J. Hydrol. 144, 335–369.
Hiscock, K.M., Tabatabai Najafi, M., 2011. Aquitard characteristics of clay-rich till deposits in East Anglia, eastern England. J. Hydrol. 405, 288–306.
Hiscock, K.M., Dennis, P.F., Saynor, P.R., Thomas, M.O., 1996. Hydrochemical and stable isotope evidence for the extent and nature of the effective Chalk aquifer of North Norfolk, UK. J. Hydrol. 180, 79–107.
Hiscock, K.M., George, M.A., Dennis, P.F., 2011. Stable isotope evidence for the hydrogeological characteristics of clay-rich till in northern East Anglia. Q. J. Eng. Geol. Hydrogeol. 44, 173–189.
Hiscock, K.M., Cooper, R.J., Lovett, A.A., Sünnenberg, G., 2023. Export coefficient modelling of nutrient neutrality to protect aquatic habitats in the River Wensum catchment. UK. Environments 10, 168. https://doi.org/10.3390/environments10100168.
Houmark-Nielsen, 2010. Extent, age and dynamics of marine isotope stage 3 glaciations in the southwestern Baltic Basin. Boreas 39, 343–359.
Husic, A., Fox, J.F., Clare, E., Mahoney, T., Zarnaghsh, A., 2023. Nitrate hysteresis as a tool for revealing storm-event dynamics and improving water quality model performance. e2022WR033180 Water Resour. Res. 59. https://doi.org/10.1029/2022WR033180.
Kawo, N.S., Korus, J., Gulbrandsen, M.L., 2023. Multiple-point statistical modelling of three-dimensional glacial aquifer heterogeneity for improved groundwater management. Hydrgeol. J. https://doi.org/10.1007/s10040-023-02658-x.
Kehew, A.E., Teller, J., 1994. History of late glacial runoff along the southwestern margin of the Laurentide Ice Sheet. Quat. Sci. Rev. 13, 859–877.
Kendall, C., 1998. Tracing nitrogen sources and cycling in catchments. In: Kendall, C., McDonnell, J.J. (Eds.), Isotope-Tracers in Catchment Hydrology. Elsevier, Amsterdam, pp. 534–569.
Kendall, C., Elliott, E.M., Wankel, S.D., 2007. Tracing anthropogenic inputs of nitrogen to ecosystems. In: Michener, R., Lajtha, K. (Eds.), Stable Isotopes in Ecology and Environmental Science, 2nd edn. Blackwell Publishing, Malden, MA, pp. 375–449.
Kessler, T.C., Klint, K.E.S., Nilsson, B., Bjerg, P.L., 2012. Characterisation of sand lenses embedded in tills. Quat. Sci. Rev. 53, 55–71.
Kessler, T.C., Comunian, A., Oriani, F., Renard, P., Nilsson, B., Klint, K.E., Bjerg, P.L., 2013. Modeling fine-scale geological heterogeneity – examples of sand lenses in tills. Groundwater 51, 692–705.
Kopáček, J., Cosby, B.J., Evans, C.D., Hruska, J., Moldan, F., Oulehle, F., Santruckova, H., Tahovska, K., Wright, R.F., 2013. Nitrogen, organic carbon and sulphur cycling in terrestrial ecosystems: linking nitrogen saturation to carbon limitation of soil microbial processes. Biogeochemistry 115, 33–51.
Ladouche, B., Probst, A., Viville, D., Idir, S., Baqué, D., Loubet, M., Probst, J.-L., Bariac, T., 2001. Hydrograph separation using isotopic, chemical and hydrological approaches (Strengbach catchment, France). J. Hydrol. 242, 255–274.
Lewis, M.A., 2014. Borehole drilling and sampling in the Wensum Demonstration Test Catchment. *British Geological Survey Commissioned Report*, CR/11/162. 52 pp.
Neuzil, C.E., 2019. Permeability of clays and shales. Annu. Rev. Earth Planet. Sci. 47, 247–273.
Meteorological Office, 2023. *UK climate averages: Coltishall 1991–2020*. Meteorological Office, Exeter. Available online at https://www.metoffice.gov.uk/research/climate/maps-and-data/uk-climate-averages/u12unggmv.
Ogunkoya, O.O., Jenkins, A., 1991. Analysis of runoff pathways and flow contributions using deuterium and stream chemistry. Hydrol. Process. 5, 271–282.
Oster, H., Sonntag, C., Münnich, K.O., 1996. Groundwater age dating with chlorofluorocarbons. Water Resour. Res. 32, 2989–3001.
Outram, F.N., Lloyd, C.E.M., Jonczyk, J., Benskin, C.M.H., Grant, F., Perks, M.T., Deasy, C., Burke, S.P., Collins, A.L., Freer, J., Haygarth, P.M., Hiscock, K.M., Johnes, P.J., Lovett, A.L., 2014. High-frequency monitoring of nitrogen and phosphorus response in three rural catchments to the end of the 2011–2012 drought in England. Hydrol. Earth Syst. Sci. 18, 3429–3448.
Outram, F.N., Cooper, R.J., Sünnenberg, G., Hiscock, K.M., Lovett, A.A., 2016. Antecedent conditions, hydrological connectivity and anthropogenic inputs: factors affecting nitrate and phosphorus transfers to agricultural headwater streams. Sci. Total Environ. 545–546, 184–199.
Patel, N., Srivastav, A.L., Patel, A., Singh, A., Singh, S.K., Chaudhary, V.K., Singh, P.K., Bhunia, B., 2022. Nitrate contamination in water resources, human health risks and its remediation through adsorption: a focused review. Environ. Sci. Pollut. Res. 29, 69137–69152. https://doi.org/10.1007/s11356-022-223772.
Peskett, L.M., Heal, K.V., MacDonald, A.M., Black, A.R., McDonnell, J.J., 2023. Land cover influence on catchment scale subsurface water storage investigated by multiple methods: implications for UK natural flood management. J. Hydrol.: Reg. Stud. 47, 101398 https://doi.org/10.1016/j.ejrh.2023.101398.
Postma, D., Boesen, C., Kristiansen, H., Larsen, F., 1991. Nitrate reduction in an unconfined sandy aquifer: water chemistry, reduction processes, and geochemical modelling. Water Resour. Res. 27, 2027–2045.
Rivett, M.O., Buss, S.R., Morgan, P., Smith, J.W.N., Bemment, C.D., 2008. Nitrate attenuation in groundwater: a review of biogeochemical controlling processes. Water Res. 42, 4215–4232.
Rowland, C.S., Morton, R.D., Carrasco, L., McShane, G., O'Neil, A.W., Wood, C.M., 2017. *Land Cover Map 2015 (25m raster, GB)*. NERC Environmental Information Data Centre. https://doi.org/10.5285/bb15e200-9349-403c-bda9-b430093807c7.
Sekar, S., Perumal, M., Roy, P.D., Ganapathy, M., Senapathi, V., Chung, S.Y., Elzain, H.E., Duraisamy, M., Kamaraj, J., 2022. A review on global status of fresh and saline groundwater discharge into the ocean. Environ. Monit. Assess. 194, 915. https://doi.org/10.1007/s10661-022-10566-y.
Sigman, D.M., Casciotti, K.L., Andreani, M., Barford, C.M.G., Böhlke, J.K., 2001. A bacterial method for the nitrogen isotopic analysis of nitrate in seawater and freshwater. Anal. Chem. 73, 4145–4153.
Steffen, W., Richardson, K., Rockström, J., Cornell, S.E., Fetzer, I., Bennett, E.M., Biggs, R., Carpenter, S.R., de Vries, W., de Wit, C.A., Folke, C., Gerten, D., Heinke, J., Mace, G.M., Persson, L.M., Ramanathan, V., Reyers, B., Sörlin, S., 2015. Planetary boundaries: guiding human development on a changing planet. Science 347, 1259855.
Sutton, M.A., Howard, C.M., Kanter, D.R., Lassaletta, L., Móring, A., Raghuram, N., Read, N., 2021. The nitrogen decade: mobilizing global action on nitrogen to 2030 and beyond. One Earth 4, 10–14.
UKCEH, 2023. *National River Flow Archive*. UK Centre for Ecology and Hydrology. Available online at: https://nrfa.ceh.ac.uk/data.

van der Kamp, G., 2001. Methods for determining the in situ hydraulic conductivity of shallow aquitards – an overview. Hydrgeol. J. 9, 5–16.

Warrack, J., Kang, M., von Sperber, C., 2022. Groundwater phosphorus concentrations: global trends and links with agriculture and oil and gas activities. Environ. Res. Lett. 17, 014014 https://doi.org/10.1088/1748-9326/ac31ef.

Webster, K.L., Leach, J.A., Houle, D., Hazlett, P.W., Emilson, E.J.S., 2021. Acidification recovery in a changing climate: observations from thirty-five years of stream chemistry monitoring in forested headwater catchments at the Turkey Lakes watershed. Ontario. *Hydrological Processes* 35, e14346.

Wexler, S.K., Hiscock, K.M., Dennis, P.F., 2011. Catchment-scale quantification of hyporheic denitrification using an isotopic and solute flux approach. Environ. Sci. Tech. 45, 3967–3973.

Wexler, S.K., 2010. *An investigation into the sources, cycling and attenuation of nitrate in an agricultural lowland catchment using stable isotopes of nitrogen and oxygen in nitrate*. PhD thesis, University of East Anglia, Norwich, UK, 397 pp.

Williams, M.R., McAfee, S.J., 2021. Water storage, mixing, and fluxes in tile-drained agricultural fields inferred from stable water isotopes. J. Hydrol. 599, 126347 https://doi.org/10.1016/j.jhydrol.2021.126347.

Wolfe, A.H., Patz, J.A., 2002. Reactive nitrogen and human health: acute and long-term implications. Ambio 31, 120–125.

Wurtsbaugh, W.A., Paerl, H.W., Dodds, W.K., 2019. Nutrients, eutrophication and harmful algal blooms along the freshwater to marine continuum. Wires Water 6, e1373.

Yuan, X., Niu, D., Guo, D., Fu, H., 2023. Responses of soil carbon and nitrogen mineralization to nitrogen addition in a semiarid grassland: the role of season. Catena 220, 106719. https://doi.org/10.1016/j.catena.2022.106719.

Zhang, A., Lei, K., Lang, Q., Yi, L., 2022. Identification of nitrogen sources and cycling along freshwater river to estuarine water continuum using multiple stable isotopes. Sci. Total Environ. 851, 158136 https://doi.org/10.1016/j.scitotenv.2022.158136.